Investigation of High Order Diffusion Models in Glioblastoma by Exploring High b-value, Echo time (TE), and Diffusion Time

by

Yuan Li

A dissertation submitted in partial fulfillment
of the requirements for the degree of
Doctor of Philosophy
(Biomedical Engineering)
in the University of Michigan
2021

Doctoral Committee:

Professor Yue Cao, Chair
Professor James Balter
Professor Jeffrey A. Fessler
Professor Douglas Noll

Yuan Li

atropa@umich.edu

ORCID iD: 0000-0003-3574-052X

Dedication

This dissertation is dedicated to my father (Hongshan Li) and mother (Jianghui Wang) who support me to pursue my dreams and finish my dissertation.

Acknowledgements

My gratitude to Yue Cao, for her guidance and support through both my masters and doctorate, and for the encouragement to pursue doctoral studies to begin with.

Thanks to the other members of my committee, James Balter, Douglas Noll, and Jeffery A. Fessler, for their insight and advice.

Additional thanks to Michelle M. Kim, Daniel Wahl, Hermant Parmar, and Theodore S. Lawrence, for their assistance, advice, and collaboration in enabling and forwarding the research presented here. Particular thanks to Daekeun You for his contributions to my research, and his camaraderie as lab mates.

This work was in part supported by NIH/NCI grant UO1 CA183848. The author thanks Siemens Healthineer for providing the providing information on diffusion gradient pulses and implementing the oscillating diffusion gradient pulses.

Table of Contents

List of Tables

List of Figures

Abstract

Glioblastoma (GBM) is the most common and aggressive primary brain tumor in adults and has a poor prognosis with a median survival of approximately 14 months. Clinical standard assessment of therapy response and tumor progression is based upon post-contrast T1-weighted (T1W) and fluid-attenuated inversion recovery (FLAIR) T2-weighted (T2W) magnetic resonance images (MRI). However, contrast enhancement observed on the post-contrast T1W MRI is affected not only by tumor growth but also effects of radiation, anti-angiogenesis drugs and chemotherapy, due to the fact that it represents blood-brain barrier disruption. Another problem is that abnormality on T2W FLAIR images is influenced by T2 changes of tumor cells as well as edema and necrosis that always co-exist within GBM. Diffusion weighted (DW) imaging has been proposed to overcome these limitations. Conventional DW images quantify apparent diffusion coefficient (ADC) with b-values between 0 and 1000 s/mm^2 using a mono-exponential decay model. One limitation is that co-existence of edema in clinical GBM elevates ADC.

In diffusion MRI, there are three dimensions of parameter spaces that we could explore in research —b value, diffusion time (t) and echo time (TE). Hence, we investigated and developed high order diffusion models in these three spaces and evaluated whether they could reveal more features of GBM.

In the b-value space, we investigated a microstructure model (MSM), in which modulation of diffusion gradient with cell size is considered, with high b-value diffusion images in the patients with GBM pre-radiation therapy (RT). We found apparent cell size (ARS), extracellular diffusion coefficient (D_{ex}) and intracellular fractional volume (V_{in}) in tumor were significantly greater than ones in normal tissue and edema. In addition, we investigated diffusion kurtosis imaging (DKI) in GBM pre-RT and mid-RT, and found pre-RT mean kurtosis of the tumor could provide a predictive value of overall survival (OS) additional to clinical prognostic factors.

In the TE space, T2-Relaxation-Diffusion correlation experiments can be powerful in resolving water compartments with respect to their size and chemical composition, but the problem is ill-posed. We simplified the T2-Relaxation-Diffusion correlation to consider the T2 values and diffusion coefficients in a correlated fashion. We found that there were significant differences between fast and slow diffusion coefficients and between associated T2 values in tumor, cortex, deep GM, and edema. Multivariate Cox model showed the fractional volume of slow component (V_s) mid-RT may add a predictive value to clinical factors.

In diffusion time space, we applied three different diffusion times using pulsed diffusion gradients (PG) and oscillating gradients at frequencies of 30 Hz (OS30) and 50 Hz (OS50) using a prototype sequence. Using a random walk with barriers model, we estimated cell diameter, unrestricted diffusion coefficient (D0) at a short time limit, bulk diffusion coefficient (D_{inf}) at a long-time limit, cell membrane permeability and effective restriction in the contrast-enhanced

tumor. Those parameters provide microstructural information in the GBM and need to be further investigated and validated with pathology.

Previous studies have mainly investigated high order diffusion models in prostate cancer and xenograft tumor models, and only a few studies investigated GBM. The current knowledge about the relationship between model parameters and physiological/pathological features in GBM are still limited. Our research in GBM could lead to better imaging means for GBM diagnosis, tumor target definition for radiation therapy, and therapy response assessment.

Chapter 1 Introduction

Glioblastoma (GBM) is the most common and aggressive primary brain tumor in adults and has a poor prognosis with a median survival of approximately 14 months despite multimodality therapy with surgery, concurrent chemoradiation therapy and adjuvant chemotherapy [1,2]. Standard clinical assessment of tumor progression or therapy response [3] is based primarily on post-contrast T1-weighted and fluid-attenuated inversion recovery (FLAIR) T2-weighted magnetic resonance images (MRI). There are some challenges to these conventional techniques. The contrast enhancement on the post-contrast T1-weighted MRI is affected by tumor growth, but also radiation, anti-angiogenesis drugs and chemotherapy, all of which can be attributed to blood-brain barrier disruption. Abnormality on T2 FLAIR images is influenced by T2 changes of tumor cells as well as edema that co-exists within GBM or is affected by radiation therapy. Limitations of conventional MRI in clinical management of GBM have motivated investigations of physiological and metabolic MRI.

Diffusion weighted (DW) imaging has been proposed to overcome these limitations. DW imaging is a technique to measure water molecule mobility in the tissue microscopic environment, and is sensitive to cell density and size, cell membrane permeability, and extracellular space tortuosity. Apparent diffusion coefficient (ADC) quantified from conventional DW images fitted to a mono-exponential function is the commonly reported

parameter in literature. The correlation between high cellularity and low ADC in tumor animal models and human cancers motivates investigations of roles of ADC in clinical GBM [4-7]. However, heterogeneous tissue in GBM, especially edema, often results in elevated ADC compared to normal white matter (WM)[1] and grey matter (GM). Another problem is that it is hard to describe the complex microstructure effects on water diffusion with a single diffusion parameter.

To deal with the deviation of diffusion weighted signals from the mono-exponential function, a bi-exponential model with fast and slow diffusion components has been proposed [8]. In the initial interpretation of the bi-exponential model, fast and slow diffusion coefficients are considered from respective extra- and intra-cellular water compartments, but the estimated fraction of the intra-cellular water in the tissue from the bi-exponential model cannot be matched with that measured by other methods [9]. The bi-exponential model fits the diffusion curves better than the mono-exponential model. A study suggests that the fast diffusion coefficient is close to the reported human brain diffusion coefficient[10]. To fit the bi-exponential model, it is necessary to acquire diffusion weighted images with more b-values, which increases the acquisition time. In addition, the bi-exponential model that fits four parameters is unstable to noise, which makes it difficult to generate high quality voxel-by-voxel brain maps.

In diffusion MRI, there are three dimensions of parameter spaces that could be explored —b value, echo time (TE) and diffusion time (t). In the b-value space, other high order diffusion models that have been investigated in tumors [11-15]. For example, a model, called VERDICT, has been proposed to quantify microstructural properties of colorectal cancer cell lines [14]. This model

considers cell size, vascular volume fraction and due to perfusion, and intracellular and extracellular fractional volumes and diffusivities. Due to the complexity of the VERDICT model, prior knowledge of intracellular and extracellular diffusion coefficients is used to fit in vivo DW images in two xenograft animal models. Another model, called the fractional order calculus model (FROC) [15], investigated diffusivity and tissue structure in brain pediatric tumor. This model requires b-values up to 4000 s/mm^2, and the diffusion coefficient in the model is pre-determined by fitting a mono-exponential model before fitting the entire model [15]. In the TE space, only a few studies were investigated [16-21]. One model, called multi-exponential proton spin-spin relaxation model [18,19], uses multi-echoes sequence to investigate multiple T2 decays in tumor and other brain tissue. White matter and gray matter showed three components and two components of T2 decay, respectively. Tumor and edema both show bi-exponentiality of relaxation time in investigation [19]. However, the fast component T2 of tumor was unexpectedly high (>700ms). Recent studies suggest that a model correlating T2 and DC together could characterize heterogeneous tissue better [16]. The capability of the 2D T2-diffusion correlation experiment to improve the sensitivity has been demonstrated on different tissue types [17,20,21]. This technique used an ill-posed equation with infinite solution [22,23], which is difficult to directly apply to diffusion curves. In the t space, previous investigators [24-27] have uncovered a time dependency of diffusion coefficient (D(t)) in many tissues, including some types of cancer. In different lengths of diffusion time, D(t) is sensitive to different microstructures, for example, membrane permeability and radius of tumor cells.

Patients with malignant gliomas experience frequent clinical complications, but glioblastoma remains a difficult cancer to treat, though therapeutic options have been improving. Optimal management requires a multidisciplinary approach and knowledge of potential complications from both the disease and its treatment [28]. T1W and T2W conventional definitions may lead to insufficient radiation dose and thereby tumor prognosis. A better definition of tumor could lead to a precision treatment, thereby a better outcome. This contribution will provide a framework for developing patient-specific models that will optimize tumor target definition for treatment planning in GBM patients.

Many studies have investigated high order diffusion models in different tumors [5,11-13,15,19,25,29-32]. However, there is very limited research in GBM with high order diffusion models, especially research that investigated in all three spaces of diffusion MRI. The current knowledge about the relationship between models and physiological features in GBM is still limited.

This work sought to investigate and develop high order diffusion models in the three spaces —b value, TE and diffusion time and evaluated whether they could reveal more physiological features of GBM.

Chapter 2 described the work that modified the model of restricted diffusion [11-13,33-35] to fit the DW images acquired with a widely available bi-polar pulse diffusion gradient imaging and characterize microstructure and diffusion properties of the hypercellular tumor in the patients with GBM. We found that fractional volume of intracellular water (V_{in}), cell radius (R) and extracellular diffusion coefficient (D_{ex}) in the tumor were substantially and significantly different from edema and normal tissue. This chapter also contains comparison with the bi-exponential

diffusion model and the ADC model. The bi-exponential diffusion model that does not explicitly model the restricted diffusion of intracellular water could not robustly differentiate GBM from edema and normal brain tissue. ADC that ignores intra-voxel heterogeneous diffusion in brain tissue and tumor failed to differentiate GBM from edema and normal tissue.

Chapter 3 investigated the diffusion kurtosis model and characterized non-Gaussian diffusion properties in the Gadolinium enhanced gross tumor volume (Gd-GTV) pre-RT and mid-RT in the patients with GBM. We found that the mean kurtosis value in the Gd-GTV pre-RT was significantly prognostic of OS as a high mean kurtosis was associated with inferior survival. Also, the diffusion kurtosis added predictive value to clinical factors for survival. In addition to glioma grading found by others previously[29,32,36], the kurtosis model has promise to aid conventional MRI for outcome prognosis.

Chapter 4 described a work that simplified the T2-Relaxation-Diffusion correlation [16] to fit the DW images and characterize diffusion properties of the hypercellular tumor in the patients with GBM. In investigation, we found that modeling T2 and DC together helps differentiate tumor from edema and normal tissue. Parameters estimated from T2-relaxation-diffusion model, such as T2 with the large diffusion coefficient ($T2_f$) and fractional volume of water with the small diffusion coefficient (V_s), correlated with PFS and show the potential to predict survival. Additionally, in our analysis of Cox proportional hazard model, pre-RT $T2_f$ and mid-RT V_s are significantly associated with reduced PFS. $T2_f$ and V_s may add value to clinical factors and aid prognosis.

Chapter 5 combined the random walk barrier model [27] (RWBM) and oscillating diffusion gradients which provide access to short diffusion times to investigate time-dependent diffusion coefficients. The RWBM model yields cell diameter, unrestricted diffusion coefficient (D_0) at a short time limit, bulk diffusion coefficient (D_{inf}) at a long-time limit, and membrane permeability (κ), which cannot be obtained by analyzing DW images with a single diffusion time. This chapter also investigated three-distance diffusion model [37] and compared it to the RWBM.

In the final chapter, implication of these investigations in GBM is discussed.

Table 1-1 Table of abbreviations appearing in text with corresponding definitions

Definition	Abbreviation
Apparent diffusion coefficient	ADC
Apparent restriction size of intracellular water	ARS
Bulk diffusion coefficient	D_{inf}
Cell radius	R
Cerebrospinal fluid	CSF
Diffusion coefficient	DC
Diffusion sensitive signals of intracellular water	S_{in}
Diffusion sensitive signals of extracellular water	S_{ex}
Diffusion tensor imaging	DTI
Diffusion weighted	DW
Diffusion weighted imaging	DWI
Echo Time	TE
Extent of surgery	EOR
Extracellular diffusion coefficient	D_{ex}
Fluid-attenuated inversion recovery T2-weighted	FLAIR T2W
Fractional anisotropy	FA
Fractional volume of intracellular water	V_{in}
Fractional volume of water with the small diffusion coefficient	V_s
Gadolinium enhanced gross tumor volume	Gd-GTV
Gaussian Phase Distribution	GPD
Glioblastoma	GBM
Grey matter	GM

Intracellular diffusion coefficient	D_{in}
Microstructure model	MSM
Mean squared errors	MSE
Oscillating gradient spin echo	OGSE
Oscillating gradient spin echo at frequency 30Hz	OGSE30
Oscillating gradient spin echo at frequency 50Hz	OGSE50
Overall survival	OS
Permeability	κ
Progression free survival	PFS
Pulse gradient spin echo	PGSE
Radiation therapy	RT
Random walk barrier model	RWBM
Signal-to-noise ratio	SNR
Structure length	l_s
T1-weighted	T1W
T2 with the large diffusion coefficient	$T2_f$
T2 with the small diffusion coefficient	$T2_s$
Tumor volume	TV
Unrestricted diffusion coefficient	D_0
Volumes of interest	VOI
White matter	WM

Chapter 2 Microstructure Modeling of High b-value Diffusion Weighted Images in Glioblastoma

This chapter is substantially equivalent to work that the author has already published in TOMOGRAPHY [38].

2.1 Introduction

High b-value DW images and high-order diffusion models have been explored in clinical gliomas to differentiate tumor grade and assess therapy response [8,9,15,32,36,39-42]. A few high-order diffusion models attempt to quantify microstructures in tumors [14,24,43]. For example, a model, called VERDICT, has been proposed to quantify microstructural properties of colorectal cancer cell lines [14]. This model considers cell size, vascular volume fraction and associated pseudo-diffusivity, and intracellular and extracellular fractional volumes and diffusivities. Due to the complexity of the VERDICT model, prior knowledge of intracellular and extracellular diffusion coefficients is used to fit in vivo DW images in two xenograft animal models. Another model, temporal diffusion spectroscopy, uses oscillating diffusion gradients to probe cellular structures that restrict intracellular water diffusion by assuming that intracellular water is restricted in impermeable cells[44-46]. Compared to VERDICT, this model simplifies representation of the extracellular water diffusion by reducing to a single free diffusion term, and fits four free parameters, including intracellular and extracellular water diffusivities.

Recent studies show that hypercellular tumor volumes that can be detected on the DW images with b=3000 mm^2/s in GBM have a prognostic value [47,48]. This technique used a widely available imaging technique and, as it is easily translatable, a current phase II clinical trial is underway that targets this hypercellular tumor volume with intensified radiation doses [49].

In this study, we modified the model described in Jiang et al [45,46]. and applied to clinical diffusion weighted images in patients with GBM. In our clinic, bi-polar pulse diffusion gradient waveforms and a high parallel imaging factor were used to reduce eddy current and geometric distortion in the clinical DW images, respectively. We applied the modified model to the DW images with high b-values to investigate whether there were any significant differences in the quantified microstructure parameters between the hypercellular tumors and normal tissue and edema in these patients. Similar comparisons were made for the conventional ADC and the parameters quantified from the bi-exponential model. This study was the first step to test the possibility of the application of the model quantifying microstructure parameters using a widely available diffusion technique on the clinical scanner for GBM.

2.2 Material and Methods

2.2.1 Microstructure model with bi-polar diffusion gradients

We assume the DW signal in tissue can be considered as a sum of water signals from intracellular and extracellular compartments [45]:

$$S = S_0[V_{in}S_{in} + (1 - V_{in})S_{ex}] \quad [2.1]$$

where S_0 is the total magnetization from both water compartments, V_{in} is the fraction volume of intracellular water, and S_{in} and S_{ex} are respective diffusion sensitive signals of intracellular and extracellular water. In previous investigations of restricted intracellular diffusion [14,45,50], a cell has been modeled as an impermeable sphere, which completely restricted diffusion of intracellular water molecules within the spherical space. The analytic formulae of the restricted diffusion signals have been derived for the conventional mono-polar diffusion pulse gradient spin echo (PGSE) and oscillating gradient spin echo sequences using the Gaussian Phase Distribution (GPD) approximation [14,45,50] which has been shown to have sufficient accuracy for most experimental conditions with PGSE sequences and for sphere and parallel-plane geometry assumptions [51]. Therefore, we adopt this formulation to express the restricted diffusion signal of the intracellular water as:

$$S_{in} = \frac{\gamma^2}{2} \sum_n B_n \int_0^{2\tau} dt_1 g(t_1) \int_0^{2\tau} g(t_2) \exp(-D_{in}\lambda_n |t_1 - t_2|)\, dt_2 \qquad [2.2]$$

where γ is the gyromagnetic ratio of proton spin, g(t) is the gradient waveform, D_{in} is the intracellular diffusion coefficient, and λ_n and B_n are structure dependent parameters. The analytical formulae of λ_n and B_n for the spherical geometry (provided by a previous work [35]) depend upon the radius (R) of the sphere or cylinder and the nth root of a Bessel function of the first kind. We total summed two terms in the equation. The integral in Eq [2.2] depends upon the specific gradient waveforms g(t) used in the diffusion pulse sequence. On the clinical scanner, the most used gradient waveform is the conventional mono polar PGSE, and the oscillating diffusion gradient wave forms are not typically available. However, large eddy currents generated in the mono-polar diffusion PGSE can produce artifacts on DW images.

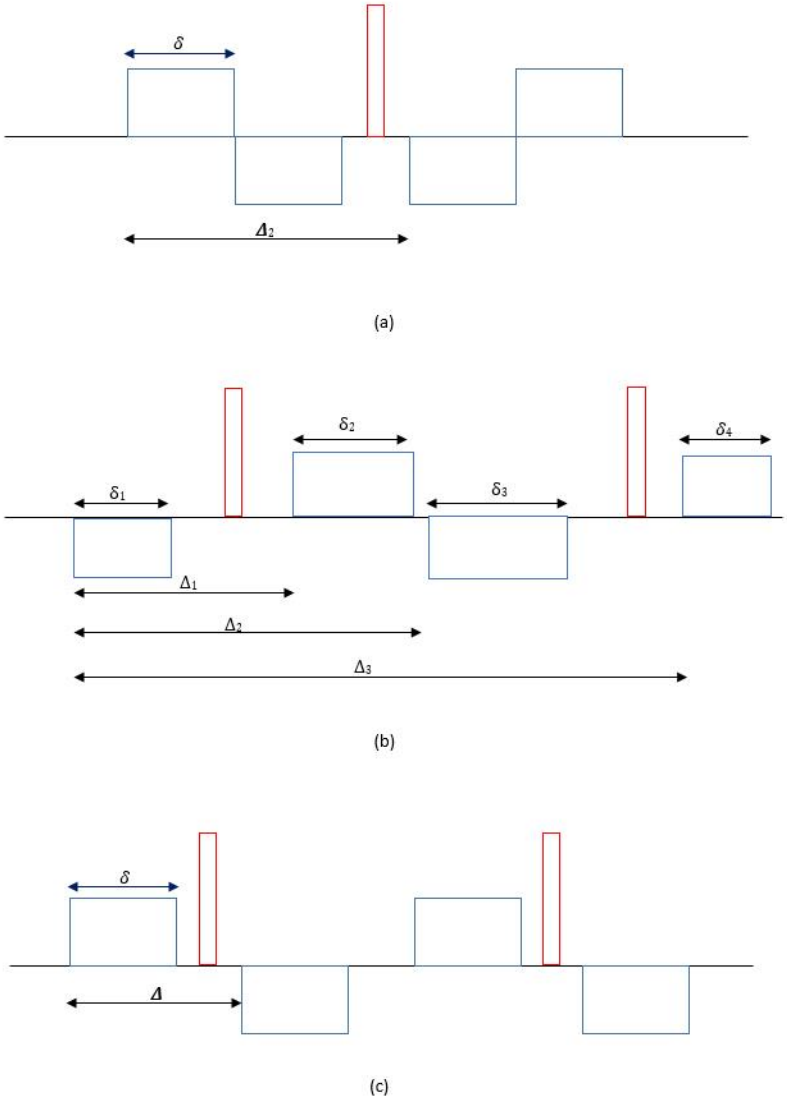

Figure 2-1 Schematic plots of three bi-polar gradient pulse waveforms. a) Symmetric bi-polar diffusion gradients are placed before and after the 180° RF pulse. b) Four gradient pulses are placed before, after and between two 180° RF pulses. Pulse durations and separations can be tuned to minimize eddy currents for a system. Therefore, all four gradient pulses durations (δ_i) and time intervals between the pulses (Δ_i) can be different. c)A special case of b. All diffusion gradient pulse durations are the same, and the gradient pulses are placed symmetrically related to the two 180° pulses.

To minimize eddy-current caused-artifacts and improve quality of DW images, bi-polar diffusion gradient pulse sequences have been introduced on clinical scanners [52]. There are a few variations in bi-polar diffusion gradient waveforms that have been implemented on the clinical

scanners by different vendors. Three common bi-polar gradient waveforms, g(t), are illustrated in Figure 2-1. The first one is introduced by Fordham et. al [53], in which bi-polar gradient pulses simply replace the mono-polar gradients before and after the 180° RF pulse. The second one contains four diffusion gradient pulses that are placed before, between and after two 180° RF pulses. The four diffusion gradient pulse durations and time intervals can be tuned to minimize eddy current effects on DW images, resulting in asymmetric waveforms (Figure 2-1b). We derived S_{in} in Eq [2.2] for three bi-polar diffusion gradient waveforms shown in Figure 2-1 and provided them in Appendix.

Finally, the extracellular diffusion signal is formulated as [45]:

$$S_{ex} = \exp(-bD_{ex}) \quad [2.3]$$

where D_{ex} is the extracellular water diffusion, and b is the b-value and depends upon the gradient waveform. For three bi-polar diffusion gradient waveforms, b-values are given in Eq [A3], [A6] and [A9] in Appendix. Note that four free parameters (R, D_{in}, D_{ex} and V_{in}) can be estimated by fitting the microstructure model (MSM) to DW images. Here, R can be considered to be an apparent restriction size (ARS) of intracellular water. Also, whether Din was sensitive to the cost function in fitting was investigated.

2.2.2 Bi-exponential model

The bi-exponential diffusion model, considered two free diffusion components, has been investigated to differentiate tumor from normal tissue and assess tumor response to therapy [54]. To compare the parameters estimated by the MSM, we implemented the bi-exponential model:

$$S = S_1 \exp(-bD_1) + S_2 \exp(-bD_2) \quad [2.4]$$

where S_1 and S_2 are respective amplitudes of apparent diffusion coefficients of D_1 and D_2. The fractional volume of water with the small diffusion coefficient is given by:

$$V_s = S_2/(S_1 + S_2) \quad [2.5]$$

Again, four free parameters (D_1, D_2, S_1, and S_2) are fitted from the bi-exponential model.

2.2.3 Conventional mono-exponential model

Conventional ADC is usually fitted to DW images with b=0 and b=1000 s/mm^2 by a mono-exponential diffusion function as:

$$S = S_0 \exp(-bADC) \quad [2.6]$$

2.2.4 Patients

Thirty patients (median age of 62 years, 19 males and 11 females) with histologically diagnosed new glioblastoma were included in this study that has been approved by an institutional review board. All patients had MRI scans post-surgery but prior to chemoradiation therapy.

2.2.5 In vivo MR imaging

All scans were performed on a 3.0-T scanner (Skyra, Siemens Healthineers) using a 20-channel head coil. Conventional MR images, 2D T2-FLAIR images, and 3D pre- and post-contrast T1-weighted images using a MPRAGE sequence, were acquired. DW images were acquired by a spin-echo echo-planar pulse sequence with diffusion weighting in 3 orthogonal directions and 11 b-values from 0 to 2500 s/mm^2 with an incremental step of 250 s/mm^2. A bi-polar diffusion gradient waveform (shown in Figure 2-1b) was used to reduce eddy currents and

improve quality of DW images. In this sequence, there were two 180^o RF pulses and four diffusion gradient pulses. The four diffusion gradient pulses had durations of δ_1=9.94ms, δ_2=15.14ms, δ_3=19.8ms, and δ_4=5.28ms. The times intervals between the first and second, the first and third, and the first and fourth gradient pulses were $\boldsymbol{\Delta}_1$=20.84ms, $\boldsymbol{\Delta}_2$=36.64ms, and $\boldsymbol{\Delta}_3$=67.34ms, respectively. Other acquisition parameters included the parallel imaging factor of 4 (GRAPPA) (to reduce echo spacing and hence geometric distortion), TE/TR=93/9300 ms, bandwidth of 1040 Hz/pixel, voxel size of approximately 1.3 x 1.3 x 5.2 mm, 30 slices to cover the whole brain, one average and total scan time of 4.50 min. It has been shown that diffusion anisotropy is lost or reduced dramatically in T2 FLAIR abnormalities of GBM due to tumor infiltration and edema [55]. To test the loss or reduction of anisotropic diffusion in GBM, DW images were also acquired in 30 directions with b=1000 s/mm^2 and 3 averages. To determine the hypercellular tumor in GBM, a diffusion image volume was acquired at b=3000 s/mm^2 and 4 averages.

2.2.6 Definition of Volumes of interest

First, we investigated whether microstructure and diffusion parameters in solid components of GBM, estimated by this model, were significantly different from ones in edema regions, normal grey matter (GM) and normal WM. Due to anticipated low SNRs in DW images, we performed this test in several volumes of interest (VOI). Previous studies of GBM using advanced imaging have shown that solid tumor components can be beyond the contrast enhanced gross tumor volumes [31,47]. Also, the T2 abnormality volume can consist of tumor, edema, and a mixture of the two. However, at high b-values, water signals of edema are

attenuated much faster than the hypercellular tumor. Based upon this hypothesis, in previous studies, a tumor volume was created by combining automated thresholding on the DW images with b=3000 s/mm^2, and then viewed and edited by a neuroradiologist with more than ten-year clinical experience [47]. The initial tumor volume was created using a threshold of the mean intensity plus 2 standard deviations calculated from a volume of interest in the normal-appearing tissue most contralateral to the T2-abnormality and performed on the DW images with b=3000 s/mm^2. Also, this tumor volume has shown to be significantly correlated with progression-free survival [47] . Therefore, we used this tumor volume (TV) to characterize microstructure and diffusion parameters by the MSM in this study. Note that this TV is different from the contrast enhanced tumor volume (Figure 2-2).

To compare the behavior of this model in edema to solid tumor in GBM, an edema volume was created within the T2-abnormality but had at least 1 cm away from both the TV used in this study and the contrast enhanced gross tumor volume. In the cases with tumor recurrence, the edema volume was checked and made sure to have no spatial overlap with the recurrent tumor volume. Also, the VOIs of two large WM fiber bundles were drawn: one in the frontal lobe and another in the Genu of corpus callosum. To compare to GM, cortex regions in the frontal and parietal lobes were segmented using the fuzzy c-means algorithm on diffusion weighted images with b=0 (T2-weighted images) and ADC maps. To avoid influence of cerebrospinal fluid (CSF), a deep GM structure, the head of caudate nucleus, was carefully chosen. As a total, six VOIs were created, see Figure 2-2.

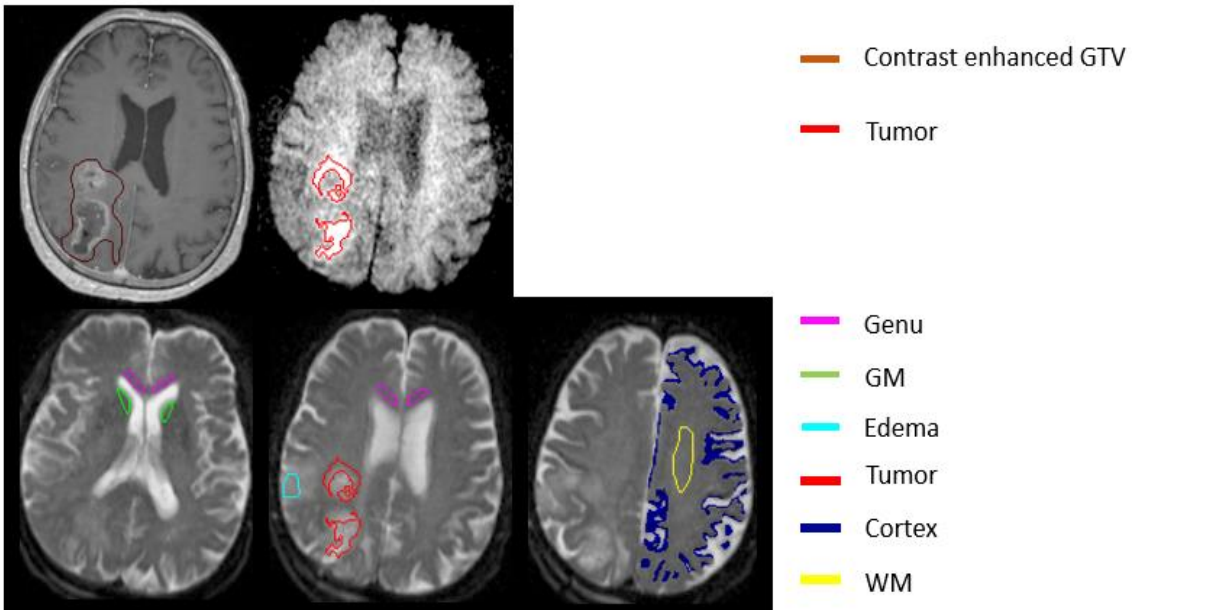

Figure 2-2 Illustration of volumes of interest (VOIs) used in the analysis. Brown contours contrast enhanced GTV on post-Gd T1W images, and red contours tumor volume on the DW images with b=3000 s/mm2. Magenta, green, cyan, blue and yellow contours represent genu, deep GM, (head of caudate nucleus), edema, cortex and frontal WM.

Before fitting the MSM, we investigated fractional anisotropy (FA) of diffusion in the defined hypercellular tumor volume (TV) to determine whether we could fit the MSM using mean diffusivities in the TV. The averaged FA was 0.15±0.05 in the TVs, which is consistent with previous reports [55], and 0.41±0.07 in the frontal WM. Therefore, it is reasonable to fit the MSM to the mean diffusion signals in the TV using a sphere assumption and omitting anisotropic diffusion. In the WM, the cylinder shape assumption was used, while the sphere shape was used in other tissue types.

Prior to the VOI creation, post-contrast T1-weighted images were reformatted into the axial plane with spatial resolution of 1x1x3 mm. All other images acquired within the same

session were reformatted to the post-contrast T1-weighted images using coordinates in the DICOM header.

2.2.7 Computation of Diffusion Models

Both the MSM and bi-exponential model were implemented using Matlab. The MSM was fitted to the DW images with 11 b-values using a *Simplex* algorithm in Matlab. We investigated the sensitivity of the objective function to the parameters of R, D_{in}, V_{in} and D_{ex}. If any parameter was not sensitive to the objective function, we would use a fixed value, which would reduce the number of the free parameters and improve the stability of fitting. *Simplex* was initiated randomly in the ranges of the parameters based on prior knowledge of the physiological parameters given in Table 2.1. Fitting was run multiple times, and the results were accepted with the minimum mean squared errors (MSE). Similarly, the bi-exponential model was fitted to the same DW images. ADC maps were calculated from DW images with b=0 and 1000 s/mm^2 using in-house Functional Image Analysis Tools (imFIAT).

Table 2-1 Ranges of Initial values of four parameters for microstructure mode fitting

Tissue type	R (μm)	D_{ex} ($\mu m^2/ms$)	V_{in}
Tumor	5-25	1-3	0-1
Normal Tissue	0.5-1.5	1-3	0-1
Edema	0.5-1.5	1-3	0-1

2.2.8 Statistical Analysis

To evaluate whether the parameters fitted from the MSM can differentiate tumor from other tissue types, Student's t-test was used and a p-value of 0.05 was considered significant. Similar analysis was applied to the parameters obtained from the bi-exponential model and ADC.

2.3 Result

2.3.1 Parameter characteristics from the MSM

When investigating sensitivity of the objective function to the parameter variation, we found that Din had little sensitivity. To test the influence of Din variations on other parameters, we varied Din from 0.1 to 1.0 $\mu m^2/ms$. We found that the fitted R in the TVs had no more than 1.5% differences, and D_{ex} and V_{in} did not show significant differences (Figure 2-3). Therefore, we fixed D_{in} at 0.1 $\mu m^2/ms$ and varied other three parameters in fitting the MSM.

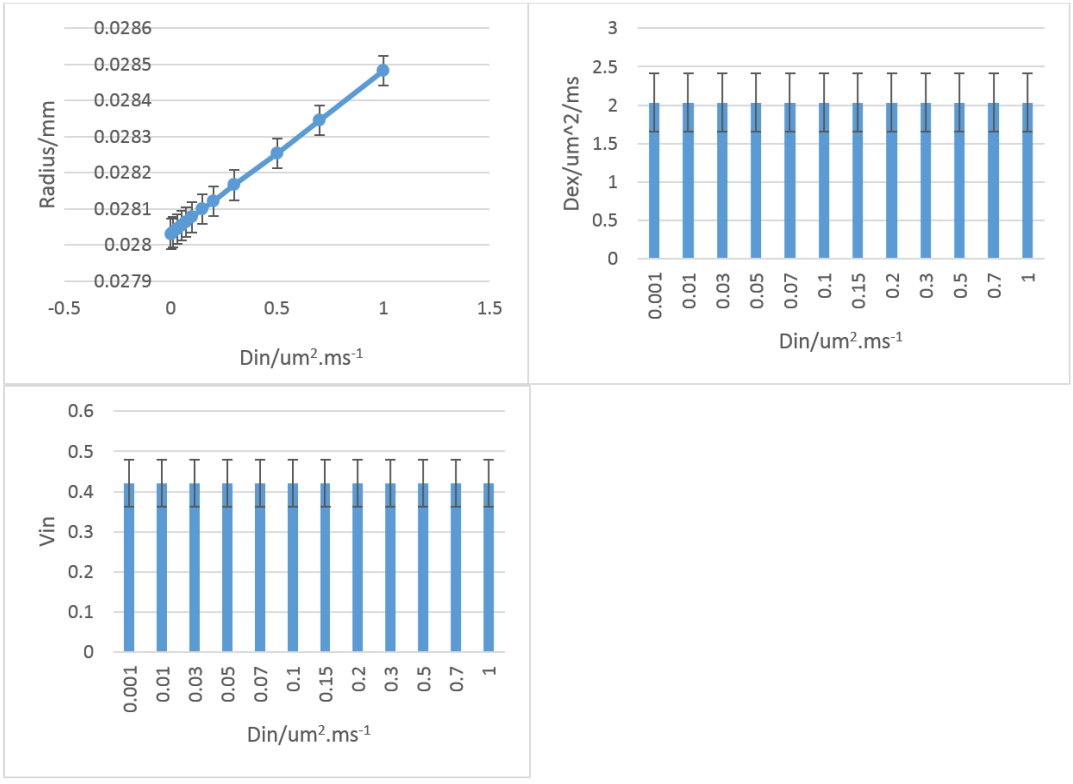

Figure 2-3 Changes in R (top left), D_{ex}(top right), V_{in}(bottom left) with D_{in} varied from 0.001 to 1 um^2/ms. Error bar is SD.

The MSM was fitted to the DW data well in all VOIs, as example curves from TV, WM, GM and edema are shown in Figure 2-4. Note that the DW signal in the TV was attenuated slower than normal GM and WM at b-values greater than 1000 s/mm^2; while the DW signal in edema was attenuated rapidly at low b-values, indicating that a large portion of extracellular water has relative free diffusion.

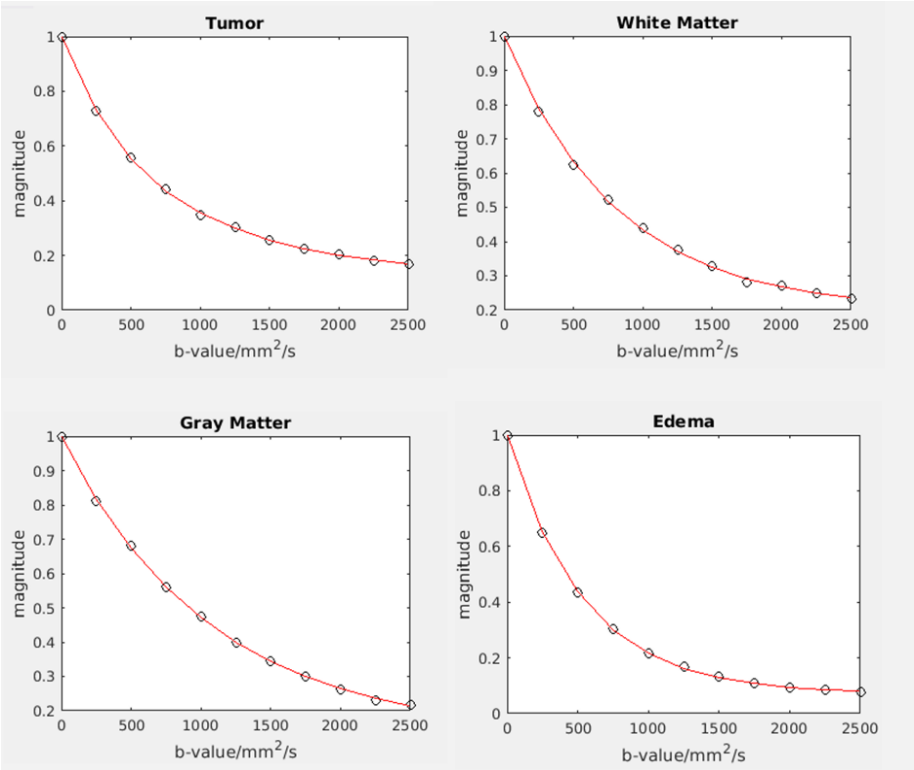

Figure 2-4 Illustration of goodness fit in tumor (top left panel), WM (top right panel), GM (bottom left panel) and edema (bottom right panel). Slide lines: fitted corves; square symbols: data points.

Characteristics of three fitted parameters in the TV, normal GM, normal WM and edema are summarized in Table 2.2 and Figure 2-5. Three parameters, R, D_{ex} and V_{in}, in the TV were significantly different from normal GM, normal WM and edema. Specifically, the mean R in the tumor was 28.1 (±0.48) μm and significantly greater than those in other tissue types (range: 1.1-

2.3 μm, $p<0.001$). In the latter group, edema had a significant greater R than normal GM and WM ($p<0.001$), which could be due to existence of a small amount of tumor cells in the edema VOI.

Table 2-2 Characteristics of Four Parameters Fitted by the Microstructure mode.

	R (um)	D_{ex}/ um^2/ms	V_{in}
Tumor	28.1±0.48	2.03±0.07	0.42±0.011
Frontal WM	1.10±0.01	1.15±0.01	0.21±0.004
Genu	1.13±0.01	1.31±0.02	0.21±0.005
Deep GM	1.19±0.05	1.19±0.04	0.16±0.004
Cortex	1.16±0.02	1.62±0.05	0.13±0.002
Edema	2.32±0.07	1.52±0.05	0.10±0.007

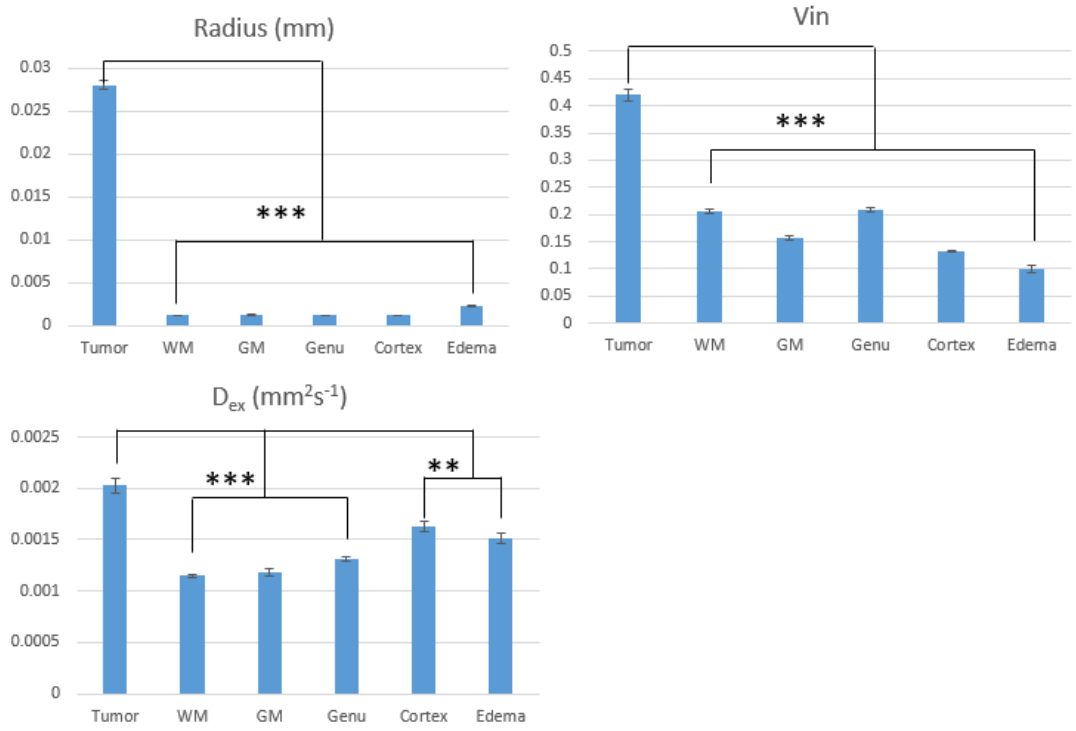

*Figure 2-5 Bar graphs of estimated parameters of R (top left panel), D_{ex} (top right panel), and V_{in} (bottom left panel) in all tissue types using the microstructure mode. **: $0.001<p<0.01$; ***: $p<0.001$. Error bar is SEM.*

The mean fractional volume of intracellular water, Vin, in the tumor was 0.42 and significantly increased compared to all other tissue types ($p<0.001$). Among normal tissue and edema, as anticipated, Vin had the highest value in the large WM fiber bundles (0.21), the intermediate values in the GM regions (0.16-0.13), and the lowest value in the edema (0.10) that is consistent with the large amount of extracellular water. Most interestingly, the values of R and Vin in the tumor had absolutely no overlap with ones in other tissue types, suggesting potential high sensitivity and specificity of R and V_{in} for differentiating tumor from edema and normal tissue.

The mean D_{ex} in the tumor was 2.03 $\mu m^2/ms$ and significantly greater than those in normal tissue and edema ($p<0.01$), which is contributed possibly from edema, micro-necrosis and perfusion mixed in the voxels of GBM. Normal WM and deep GM had D_{ex} values of 1.15 – 1.31 $\mu m^2/ms$, which is consistent with other reports [10]. Edema had D_{ex} of 1.52 $\mu m^2/ms$, largely attributing to the great fractional volume of extracellular water. Cortex had D_{ex} of 1.62 $\mu m^2/ms$, possibly resulting from partial volume average effects with cerebral spinal fluid (CSF).

2.3.2 Parameter Characteristics from the Bi-exponential Model

Characteristics of the three fitted parameters by the bi-exponential model are summarized in Table 2.3 and Figure 2-6. None of the three parameters in the tumor significantly and completely differed from the values in all other tissue types. D_1 (the large diffusion coefficient) in the tumor was 2.02±0. 07 $\mu m^2/ms$, was not significantly different from edema (1. 89±0. 06 $\mu m^2/ms$), but was significantly greater than normal WM and deep GM ($P<0.05$). Cortex had the significantly elevated D_1 compared to tumor and other normal tissue ($P<0.01$). D_2 in the tumor

was 0. 34±0.01 μm^2/ms, was not significantly different from edema (0. 33±0. 04 μm^2/ms), deep GM and cortex (0.36±0.02 μm^2/ms), but was significantly greater than normal WM (0.16-0.21 μm^2/ms, $p<0.01$). V_s in the tumor was 0.42, significantly greater than edema (0.29, $p<0.05$) and genu (0.33, $p<0.05$), and not significantly different from frontal WM and deep GM. Cortex had the highest values in D_1, D_2 and V_s than tumor and normal WM and GM, possibly due to the partial volume average with CSF and suggesting that the bi-exponential model is strongly influenced by fluid components.

Table 2-3 Characteristics of Three Parameters Fitted by the Bi-exponential Model.

	D_1 /μm^2/ms	D_2/ μm^2/ms	V_s
Tumor	2. 02±0. 07	0. 34±0. 01	0. 42±0. 01
Frontal White	1. 44±0. 03	0. 21±0. 02	0. 38±0. 01
Genu	1. 55±0. 04	0. 16±0. 02	0. 33±0. 02
Deep Gary	1. 73±0. 07	0. 36±0. 02	0. 46±0. 02
Cortex	2. 78±0. 06	0. 55±0. 01	0. 51±0. 02
Edema	1. 89±0. 06	0. 33±0. 04	0. 29±0. 04

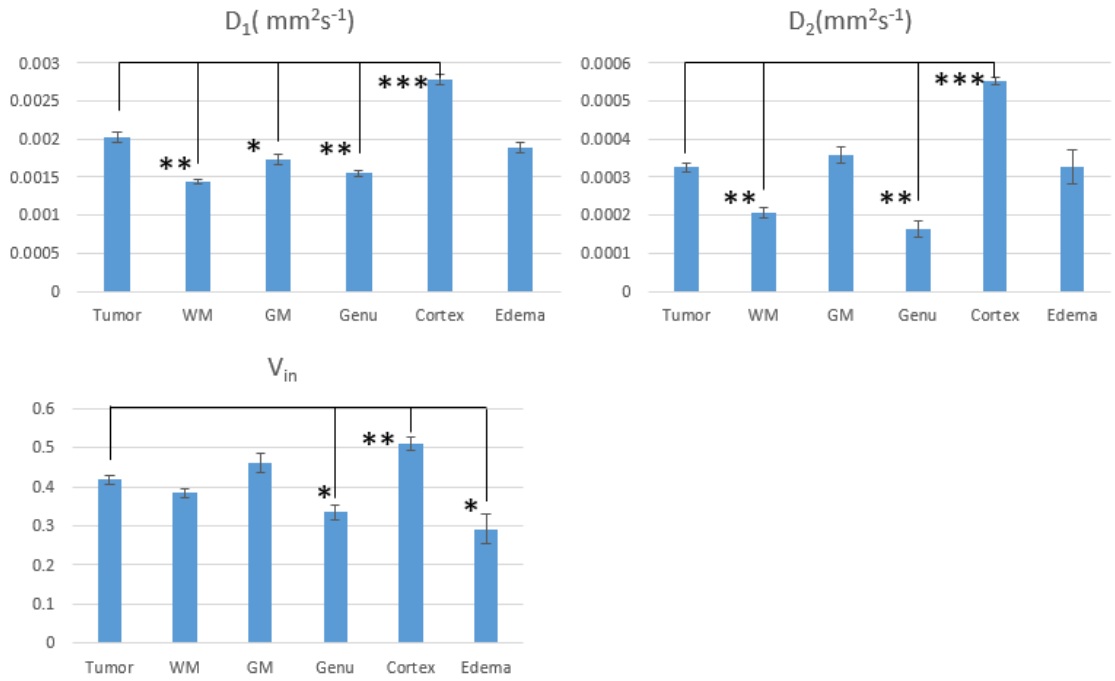

*Figure 2-6 Bar graphs of estimated parameters of D_1 (top left panel), D_2 (top right panel), and V_s (bottom left panel) in all tissue types using the bi-exponential diffusion model. *: 0.01<p<0.05; **: 0.001<p < 0.01; ***: p < 0.001. Error bar is SEM.*

To test whether combining all three parameters (D_1, D_2 and V_s) could differentiate tumor from all other tissue types, binary multivariate logistic regression was applied to the data. Backward rejection with p>0.1 was used to eliminate the parameters in the logistic regression models. In the first model including the three parameters (Table 2.4), D_1 was significant ($p < 0.05$), but V_s was not significant and D_2 was marginally significant. However, D2 had a large negative coefficient that could offset the D_1 contribution in the model. In the second model where V_s was rejected, D_1 was marginally significant, and D_2 was not significant. In the final model, D_1 was not significant after rejecting D_2.

Table 2-4 Multi-variate Logistic Regression Using the Parameters from the Bi-exponential Model.

First	D1	D2	Vs
Coefficient	1215.93	-5009.1	3.55
P value	0.04	0.06	0.16
Second	**D1**	**D2**	
Coefficient	975.2	-2327.3	
P value	0.075	0.19	
Third	**D1**		
Coefficient	428.6		
P value	0.23		

2.3.3 Conventional ADC Model

There were no significant differences of ADC between tumor and any other non-tumor tissue types ($p>0.05$) (Figure 2-7). In general, ADC in the tumor was greater than WM and deep GM but lower than edema and cortex, consistent with other reports (7).

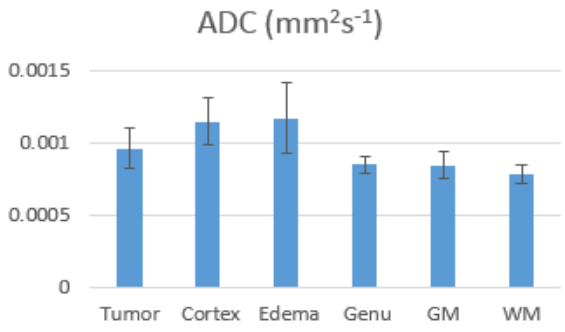

Figure 2-7 Bar graph of apparent diffusion coefficients in all tissue types using the mono-exponential diffusion model. Error bar is SEM.

2.4 Discussion

In this study, we modified the model of [11,12,33-35,45]to fit the DW images acquired with a widely-available bi-polar pulse diffusion gradient imaging and characterize microstructure and diffusion properties of the hypercellular tumor in the patients with GBM. We found that three

parameters (V_{in}, R and D_{ex}) in the tumor were substantially and significantly different from edema and normal tissue. The bi-exponential diffusion model that does not explicitly model the restricted diffusion of intracellular water could not robustly differentiate GBM from edema and normal brain tissue. ADC that ignores intra-voxel heterogeneous diffusion in brain tissue and tumor failed to differentiate GBM from edema and normal tissue. The Microstructure model has a great promise to aid in to conventional MRI for GBM diagnosis, image-guide therapy and response assessment. Further validation with histopathology will warrant the role of the microstructure mode in the clinical management of GBM.

In the current study, the fractional volume of intracellular water, V_{in}, in GBM estimated by the microstructure model was found substantially different from edema and normal tissue. The V_{in} in the TV had the largest value, which makes possible to differentiate the GBM from surrounding tissue. Also, GBM has enlarged cell size and nucleus, and increased cell density, which can increase Vin measured in image voxels, and has micro-necrosis and edema, which can reduce V_{in} [56,57]. In the current study, the estimated V_{in} in GBM by the microstructure model was 1.75-fold greater than one reported in a previous study that included primary and metastatic cancers and used the bi-exponential diffusion model [13]. Historically, the bi-exponential diffusion model often results in an underestimated Vin, for which several possible causes have been discussed [10]. The underestimation in Vin can be caused by the transcytolemmal water exchange that is omitted in the model as well as low SNR in DW images [58]. Also, T2 differences between intracellular and extracellular water could affect the estimated Vin values, which will be discussed further in the last paragraph. Diffusion gradient, b-value range, diffusion model, and

subject age all have influence on the estimated V_{in} [7]. As expected, the lowest V_{in} value was found in edema, consistent with the notion of a large amount of extracellular water in the region. The V_{in} values in two large WM fiber bundles and GM are between the solid GBM and edema, suggesting that the MSM has the potential to differentiate the GBM from surrounding tissue. In this study, we evaluated anisotropic diffusion in the hypercellular tumor volume and found low FA (0.15 as a mean value). Therefore, we did not consider anisotropic diffusion in the MSM. In the future study, anisotropic diffusion could be considered in the microstructure model.

Our microstructure model yielded the substantial greater R in GBM than in normal GM, normal WM, and edema. R could be considered as the apparent restriction size of intracellular water and a possible biomarker to differentiate GBM from normal tissue. The R value should be considered as an average value over a distribution. Previous studies have shown the increased radius of tumor cells compared to normal tissue using the microstructure model or VERDICT model, and the reasonably correlation between the DW image estimated cellularity and histopathologically determined cellularity [14,44]. A pathological study in GBM shows that the radius of GBM cells can be as large as 20 μm with a mean of 10 μm and a standard deviation of 11 μm [59]. The size of the apparent restriction space estimated in our model is larger than the reported cell size. Many factors can cause an overestimation in the restriction size of intracellular water in GBM. It is most likely that the highly permeable cell membrane cannot restrict intra-cellular water diffusion like a hard boundary. As a result, the soft boundary increases the estimated radius so that we could call the estimated radius from our MSM as an effective radius. The low SNR in DW images could further cause an overestimate of R [60]. Due

to the diffuse nature of GBM, diffused tumor cells can be found in the edema region [61,62], which could be the cause of the slight but significant increase in the apparent restriction size in the edema region. Further studies could be carried out to investigate whether combining R and Vin in the image voxels with edema can provide information on the GBM cell infiltration and distribution.

In the current study, the value of D_{ex} in GBM by the microstructure model was found significantly greater than those in normal GM, normal WM and edema, which is similar to one by the bi-exponential diffusion model (Table 2.3), and also consistent with the values reported by Mulkern et al. [10]. Dex in GBM is affected by the large quantity of extracellular water due to co-existence of edema, and to a small extent by micro-necrosis and perfusion (40). To reduce the number of free parameters in the model, we did not account for the perfusion-cause pseudo diffusion in D_{ex}. However, we have tested the perfusion effect on D_{ex} in the TV VOIs in 30 patients using the approach in [63]. We estimated that the pseudo diffusion coefficient was approximately 0.15 $\mu m^2/ms$, which was 13.5 times smaller than D_{ex} (2.03 $\mu m^2/ms$) in the tumor VOIs. Thus, in the TV VOIs defined in our study, omitting the perfusion effect did not cause a substantial overestimate in D_{ex}. Note that the TV VOI used in our study is not the contrast enhanced tumor volume. We believe that the high D_{ex} in GBM could be mainly due to edema. The relative high values of D_{ex} in cortex and edema are likely due to the partial volume average of CSF in the cortex VOI, and the large amount of extracellular water in the edema region, respectively.

As discussed in Introduction, modeling microstructure and diffusion properties in tumors has been attempted by different models [24,43,45,50,60]. In general, these models fit more free parameters and require long acquisition times. The signal-to-noise ratio (SNR) of DW images is also a limiting factor to produce robust fitted parameters. Furthermore, there are great time restriction, technology availability, and other practical considerations when acquiring diffusion weighted images in the patients with GBM on a clinical scanner. For example, we used a bi-polar pulse diffusion gradient waveform to reduce eddy-current induced artifacts and a high parallel imaging factor to improve geometrics accuracy. With these acquisition limitations, we modified and tested the model in reference [11,45] using the widely available technology on a clinical scanner in the patients with GBM. For other bi-polar diffusion gradient waveforms, we provided equations of the model in Appendix.

The MSM demonstrated the prognostic potential and also the opportunity to better distinguish GBM from normal tissue and edema. However, the current study has a few limitations. First, our sample size is not large, with only 30 patients. This could result in overfitting. The MSM needs to be further validated in an independent large cohort of patients in future. Second, the restriction space of intracellular water is modeled as an impermeable sphere, which has been used in both VERDICT and temporal diffusion spectroscopy model [14,44,50]. A previous simulation work suggests that omitting water exchange at the boundary of the restriction space of water diffusion leads to an underestimation of Vin but has little influence on the estimation of the space size [60]. Whether omitting the permeability of cell membrane or restriction space could lead to an overestimation or underestimation of the size of the restriction

space in GBM needs a further investigation. Anisotropic diffusion was not considered in this study, which could be considered in the future work, particularly for the regions with tumor cell infiltration. Nevertheless, the microstructure model using a clinically available diffusion pulse sequence leads to a better differentiation between the hypercellular tumor and normal tissue or edema than the bi-exponential and mono-exponential models.

Chapter 3 Survival Prediction Analysis in Glioblastoma with Diffusion Kurtosis Imaging

This chapter is substantially equivalent to work that was published in Frontiers in Oncology[64].

3.1 Introduction

Diffusion tensor imaging (DTI) is an emerging technique to investigate brain tumor. Fractional anisotropy (FA) that derived from DTI has been suggested to provide information of cell density. A previous study of FA in GBM showed that FA was low in GBM and suggested that the directional diffusion has been corrupted in the tumor region [38]. However, how to differentiate low FA caused by tumor from that affected by edema is a challenge.

The signal-to-noise ratio of diffusion weighted images acquired on clinical scanners is a limiting factor to apply the high-order diffusion models to GBM. Diffusion kurtosis imaging (DKI) is an emerging approach to estimate the non-Gaussian water diffusion behavior over high b values in tissue. DKI has shown the potential to characterize normal and pathologic tissue [36,65]. Previous research has suggested that DKI provides better separation of brain tumor grades [29], but there are very limited efforts in investigating treatment responses of kurtosis in GBM and its prognostic and predictive values for patient survival [66].

In this study, we hypothesized that high diffusion kurtosis in GBM correlated with decreased overall survival (OS). We applied the diffusion kurtosis model to the DW images acquired in the patients with GBM before radiation therapy (pre-RT) and during the course of

RT (mid-RT). We analyzed the parameter differences in pre-RT, mid-RT and post-RT to investigate the bio-physical meaning of the parameters and response to RT. Finally, we tested whether any parameter derived from the model is a significant predictor of progression free survival (PFS) and OS.

3.2 Material and Methods

3.2.1. Patients

Thirty-three patients with histologically confirmed, newly diagnosed GBM were enrolled on prospective, institute-review-board approved protocols. All patients signed written informed consents. The patients had research MRI scans, including anatomic scans and diffusion weighted (DW) images, pre-RT following maximal tumor surgical resection prior to chemo-radiation therapy (CRT) and during the 3rd-4th week of CRT (mid-RT). Twenty-one patients had the research MRI scans 3-month post-RT. Ten patients were treated based upon the institution protocol of concurrent CRT following chemotherapy with a median dose of 60 Gy (40.05-72 Gy), and 23 patients were enrolled on a prospective radiation boosting clinical trial and treated to 75 Gy (NCT02805179) [67]. All patients received concurrent temozolomide.

3.2.2. In Vivo MR Imaging

All MRI scans were performed on a 3.0-T scanner (Skyra, Siemens Healthineers) using a 20-channel head coil. Conventional MR images, 2D T2-FLAIR images, and 3D pre- and post-contrast T1-weighted images using a MPRAGE sequence, were acquired. DW images were acquired by a spin-echo echo-planar pulse sequence with diffusion weighting in 3 orthogonal

directions and 11 b-values from 0 to 2500 s/mm^2 with an incremental step of 250 s/mm^2. Other acquisition parameters included a parallel imaging factor of 4 (GRAPPA) (to reduce echo spacing and hence geometric distortion), TE/TR=93/9300 ms, bandwidth of 1040 Hz/pixel, voxel size of approximately 1.3 x 1.3 x 5.2 mm, 30 slices to cover the whole brain, one average and total scan time of 4.50 min. All DW images were acquired prior to contrast injection.

3.2.3. Diffusion Model

The diffusion kurtosis model analyzes non-Gaussian water diffusivity with equation [68]:

$$S = S_0 * e^{(-b*D+\frac{1}{6}(b*D)^2*K)} \quad (1)$$

where S_0 is an amplitude of diffusion signals, which is a fixed value for every b-value. D is a diffusion coefficient (DC) that is corrected for the observed non-Gaussian diffusion behavior and K represents an apparent diffusional kurtosis. Here, we did not consider an anisotropic diffusion kurtosis in GBM due to the low anisotropic diffusion behavior in the contrast-enhanced tumor volume.

3.2.4. Computation of Kurtosis and DC Maps

Kurtosis and DC maps were generated from DW images with 11 b-values using in-house Functional Image Analysis Tools (imFIAT). We first took a logarithm of diffusion signals, and then used Simplex algorithm to fit the model. In the computation process, a 2D 3x3 Gaussian filter and brain mask were first applied to all phases of diffusion weighted images to reduce noise influence on the parameter maps.

The gadolinium enhancement gross tumor volumes (Gd-GTV) on post-Gd T1 weighted images were delineated by radiation oncologists who treated the patients. Surgical cavities were removed from the Gd-GTV. The median of the residual Gd-GTV is 20.97 cm^3 (ranges from 2.33 to 62.50 cm^3). In eighteen patients with gross total resection (Table 1), the median of the residual Gd-GTV (excluding the surgical cavity) was 14.00 cm^3 (ranges from 2.33 to 46.00 cm^3).

Considering GBM is a heterogeneous tumor with edema (possible low cellular density) and high cellular components, a mean value of kurtosis or diffusion coefficient averaged over the whole volume of Gd-GTV-cavity could wash out the component that could be more aggressive and predict outcomes. Therefore, we attempted to analyze the part of the histogram of kurtosis or diffusion coefficient, which is associated with the aggressive tumor. Since high kurtosis values and low diffusion coefficients are associated with tumor aggressiveness, we choose high percentiles of kurtosis and low percentiles of DC to test whether they predicted OS. Therefore, mean, 80 percentile and 90 percentile values of kurtosis, and mean, 10 percentile and 20 percentile values of DC in the Gd-GTV pre-RT and mid-RT were calculated.

3.2.5. Statistical Analysis

The primary endpoint of the study was to determine whether the DKI parameters provide additional predictive values over clinical variables for OS. OS was defined as the interval from the start of RT to death from any cause. Patients were censored at the time of last contact or clinical follow-up, whichever occurred last. Patients were generally followed every 8 weeks after chemoradiation with clinical exam and MRI. Progression-free survival (PFS) was defined as the interval from the start of RT to progression or death, whichever occurred first, and patients were

censored at the time of last imaging follow-up. Progression was determined by a multidisciplinary tumor board, and worsened enhancement within 3 months of chemoradiation was generally managed by repeat imaging to rule out pseudo-progression. Progression was defined as worsened enhancement outside of the radiation field, or within the radiation field if progression was confirmed pathologically or with serial confirmatory imaging and clinical evaluation, or by change in therapy (i.e. initiation of next-line chemotherapy), whichever occurred first.

PFS and OS were calculated using Kaplan-Meier method. To test predictive values of the DKI parameters, univariate Cox proportional hazards model first was used to evaluate each of the DKI parameters as well as clinical factors for prediction of OS and PFS.

GBM is a heterogeneous tumor with edema (possible low cellular density) and high cellular components. A mean value of kurtosis or diffusion coefficient averaged over the whole volume of Gd-GTV-cavity could wash out the component that could be more aggressive and predict outcomes. Therefore, we attempted to analyze the part of the histogram of kurtosis or diffusion coefficient, which is associated with the aggressive tumor. Considering that high kurtosis values and low diffusion coefficients are associated with tumor aggressiveness, we choose high percentiles of kurtosis and low percentiles of DC to test whether they predicted OS. Clinical factors included age (continuous), sex, ECOG performance status (0 vs 1 vs 2), radiation dose (continuous), extent of resection (EOR, gross total resection=2, subtotal resection=1, or biopsy=0), MGMT methylation status (methylated vs unmethylated), and baseline contrast enhanced gross tumor volume (GTV-Gd). Multivariate Cox proportional hazards model was

further performed to test whether the DKI parameters could provide additional values to clinical factors for prediction of OS and PFS, adjusting age, MGMT methylation status and EOR. The changes in the DKI parameters at mid-RT compared to pre-RT were also tested using a paired t test. A P-value < 0.05 was considered significant.

3.3 Results

3.3.1. Patient Characteristics and Outcomes

Thirty-three patients who had newly diagnosed GBM treated between October 2012 and December 2018 and had the diffusion imaging scans pre-RT and mid-RT as described in 2.2 were included in this analysis. The patient characteristics are provided in Table 1. The median age was 61 years old (50-79). Thirteen patients were female. Thirty patients ECOG performance status were 0-1. Eighteen patients had total surgical resection, 9 had subtotal resection and 6 had biopsy only. Eight of the 31 patients who had MGMT methylation tests were methylated, and one of the 32 patients who had IDH tests had the mutated type.

Table 3-1 Patients characteristics.

Count	N
Patients	33
Age	
Median (IQR)	61 (50, 79)
Gender	
Female	13 (39.4%)
Male	20 (60.6%)
ECOG	
0	7 (21.2%)
1	23 (69.7%)
2	3 (9.1%)

Median Physical Dose	
Institute Protocol	60 (40.05, 72)
Boosting Protocol	75 (75, 75)
Extent of Surgery	
Biopsy	6 (18.2%)
Subtotal resection	9 (27.3%)
Gross total resection	18 (54.5%)
MGMT Methylation	
Positive	9 (27.2%)
Negative	22 (66.7%)
Unknown	2 (6.1%)
IDH Status	
Mutant	1 (3%)
Wild Type	31 (94%)
Unknown	1 (3%)

The 14 of patients were still alive with a median followup of 17.4 months (9.07-49.4 months). The median survival was 13.7 months (0.6-37.5 months). The 25 patients were progressed with a median progression of 8 months (0.6-25 months), with one patient progressed (3 weeks) at mid-RT. Figure 1 shows Kaplan-Meier curves of OS and PFS.

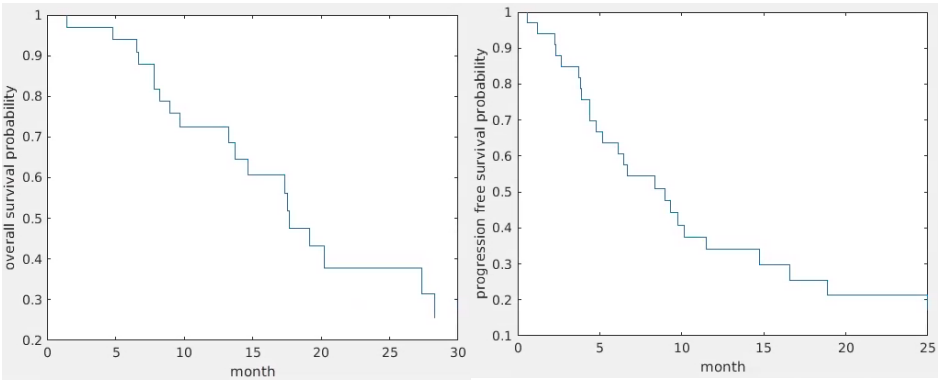

Figure 3-1 Kaplan-Meier curves of OS (left) and PFS (right).

3.3.2 Kurtosis and DC values in the Gd-GTV pre-RT, mid-RT and psot-RT

Kurtosis and DC maps of the 33 patients pre-RT and mid-RT were calculated, and an example of kurtosis maps and the diffusion curve in the Gd-GTV is shown in Figure 2. Note that the kurtosis values in the Gd-GTV were heterogeneous. We investigated the mean kurtosis values in the Gd-GTV as well as the 80 percentile and 90 percentile values pre-RT and mid-RT. Similarly, we investigated the mean DC, 10 percentile and 20 percentile values in the Gd-GTV pre-RT and mid-RT. All data are summarized in Table 2.

Figure 3-2 Illustration of a kurtosis map (color-coded, middle) of a patient with GBM. The color bar indicates kurtosis values. The post-Gd tumor volume (Gd-GTV, red contour) delineated on T1-weighted images (left) is overlaid on the kurtosis map. An example of diffusion weighted signals fitted by the diffusion kurtosis model is shown in the right panel. Blue dots represent original diffusion signal data in the Gd-GTV, and red solid line is the fitted curve. Note that the diffusion kurtosis model fits the diffusion signals well.

Table 3-2 Kurtosis and DC values in the Gd-GTV pre-RT, mid-RT and post-RT.

	Pre-RT	**Mid-RT**	**Post-RT**
Mean Kurtosis ± SD	0.76 ± 0.10	0.73 ± 0.18	0.65 ± 0.14
80 percentile Kurtosis ±	1.07 ± 0.18	0.98 ± 0.27	1.04 ± 0.67
90 percentile Kurtosis ±	1.18 ± 0.24	1.07 ± 0.31	1.23 ± 1.04
Mean DC ($\mu m^2/ms$) ± SD	1.54 ± 0.30	1.67 ± 0.34	1.71 ± 0.43
10 percentile DC (um^2/ms)	0.89 ± 0.13	1.07 ± 0.17	1.81 ± 0.47
20 percentile DC(um^2/ms)	1.02 ± 0.15	1.20 ± 0.20	1.89 ± 0.51

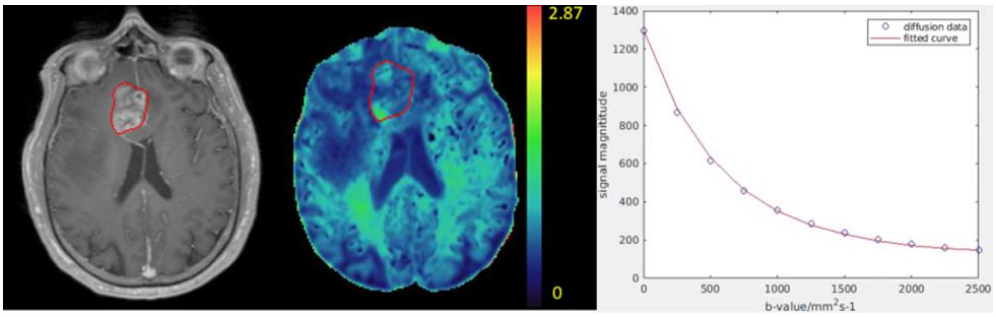

The kurtosis values and DC values in the Gd-GTV at mid-RT were decreased and increased significantly (P value<0.005) compared to pre-RT, respectively (Figure 3). The three

outlier data points in the kurtosis plot that did not follow the decrease group treads from pre-RT to mid-RT were from one patient who had rapid progression after treatment. In the DC plot, five outliers deviated from the group trend came from three patients and were due to necrosis, tumor infiltrated in the ventricle or adjacent to the surgical cavity.

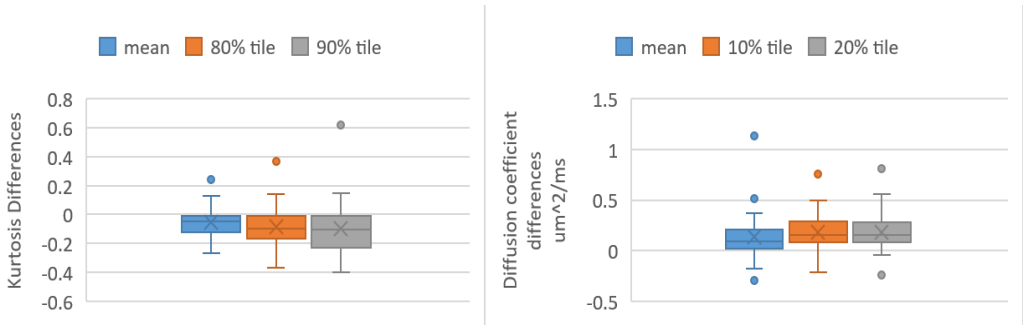

Figure 3-3 Box and whisker plots shows values of kurtosis differences and DC differences in Gd-GTV pre-RT and mid-RT (mid-RT values – pre-RT values). Left one is kurtosis differences of mean, 80 percentile and 90 percentile kurtosis values. Right one is DC differences of mean, 10 percentile and 20 percentile DC values.

The post-RT mean kurtosis, 80 percentile and 90 percentile values, and mean DC, 10 percentile and 20 percentile values in the Gd-GTV of the 21 patients are summarized in Table 2. Note that the post-RT mean kurtosis and DC values continued decreasing and increasing from the values from mid-RT, respectively. The large variances of kurtosis and DC over the group could be due to progression observed in two patients at 3 months post-RT.

3.3.3 Correlation of parameters with OS and PFS

Univariate Cox model analysis showed that large mean, 80 percentile, and 90 percentile kurtosis values in the Gd-GTV pre-RT were significantly associated with reduced OS (respective HR=2.10, p=0.03; HR=2.29, p=0.03; and HR=2.30, p=0.03; Table 4), but not the values

measured at mid-RT (p value >0.83) and post-RT (p value >0.47). The DC values including the mean, 10 percentile and 20 percentile from the Gd-GTV pre-RT, mid-RT and post-RT did not show any significant association with OS (p value >0.3). Univariate Cox model analysis of clinical prognostic factors and dose for prediction of OS are listed in Table 3.

We further addressed the question whether kurtosis values in the Gd-GTV added any values than clinical prognostic factors, such as EOR, age, MGMT and Gd-GTV, for prediction of OS. Due to the similarity that exists among mean, 80 percentile, and 90-percentile kurtosis values in the Gd-GTV, we only selected the mean kurtosis in the analysis. After adjusting these clinical factors, the mean kurtosis value pre-RT was a significant predictor of OS (HR=3.06, p<0.009), see Table 4.

The mean, 80 percentile and 90 percentile kurtosis values and the DC values in the Gd-GTV pre-RT and mid-RT were not significant predictors for PFS (p>0.5) using univariate Cox model analysis. However, the post-RT values of kurtosis, specifically, the large values of kurtosis at the 80 percentile and 90 percentile in the Gd-GTV were associated with reduced PFS in the univariate Cox model analysis (p=0.03 and p=0.05, respectively), see Table 5, which could be a useful indicator for time of progression.

Table 3-3 Univariate Cox model analysis of DKI parameters and clinical factors for prediction of OS

Parameters	Hazard ratio (HR)	p-value	95% CI
Mean K pre-RT	2.10	0.03*	[1.10, 4.02]
80 percentile K pre-RT	2.29	0.03*	[1.10, 4.71]
90 percentile K pre-RT	2.30	0.03*	[1.07, 4.96]
Gd-GTV pre-RT	0.74	0.25	[0.44, 1.23]
Age	1.72	0.14	[0.84, 3.52]
MGMT	0.45	0.2	[0.14, 1.47]

Dose	1.20	0.07	[0.98, 1.46]
EOR	0.34	0.52	[0.63,2.52]

**: significant with p <0.05. The continuous data were normalized.*

Table 3-4 Multivariate cox model analysis of clinical factors and MK for prediction of OS

parameters	Hazard ratio (HR)	p-value	95% CI
Age	2.92	0.03*	[1.08, 7.94]
MGMT	0.25	0.09	[0.05, 1.24]
EOR	0.55	0.21	[0.21, 1.42]
mean K pre-RT	3.06	0.009*	[1.32,7.13]

**: significant with p <0.05. The continuous variables were normalized.*

Table 3-5 Univariate Cox model analysis of DKI parameters post-RT for prediction of PFS

Parameters	Hazard ratio (HR)	p-value	95% CI
Mean K post-RT	1.85	0.10	[0.88, 3.88]
80-percentile K post-RT	2.18	0.03*	[1.10, 4.30]
90-percentile K post-RT	1.82	0.05*	[1.00, 3.33]

**: significant with p <0.05. The continuous variables were normalized.*

3.4 Discussion

In this study, we investigated the diffusion kurtosis model and characterized non-Gaussian diffusion properties in the Gd-GTVs pre-RT and mid-RT in the patients with GBM. We found that the mean kurtosis value in the Gd-GTV pre-RT was significantly prognostic of OS as a high mean kurtosis was associated with inferior of survival. Also, the diffusion kurtosis added a predictive value to the extent of surgery, age and methylation status for survival. The post-RT kurtosis values in the Gd-GTV predicted time to progression. In addition to glioma grading [29,32,36], kurtosis model has promise to aid in to conventional MRI for outcome prognosis. Further validation with another cohort of patients will warrant the role of the diffusion kurtosis model in the clinical management of GBM.

Many diffusion models have been investigated in gliomas. An apparent diffusion coefficient quantified from conventional DW images with b-values between 0 and 1000 s/mm^2 using a mono-exponential decay is the commonly reported parameter in literature. Previous studies have suggested that a low ADC was associated with a decrease in survival for patients with gliomas [30,69-72]. One limitation of the mono-exponential model is that there are large deviations of fitted curves from the diffusion weighted signals with b-values greater than 1500 s/mm^2. Another problem is that with a single diffusion parameter is hard to describe the complex microstructure effects on water diffusion. To deal with the deviation of diffusion weighted signals from the mono-exponential function, a bi-exponential model with fast and slow diffusion components has been proposed [8]. In the initial interpretation of the bi-exponential model, fast and slow diffusion coefficients are considered from respective extra- and intra-cellular water compartments, but the estimated fraction of the intra-cellular water in the tissue from the bi-exponential model cannot be matched with that measured by other methods [9]. The bi-exponential model fits the diffusion curves better than the mono-exponential model. A study suggests that the fast diffusion coefficient is close to the reported human brain diffusion coefficient [10]. To fit the bi-exponential model, it is necessary to take diffusion weighted images with more b-values, which increases the acquisition time. In addition, the bi-exponential model that fits four parameters is unstable to noise, which makes it difficult to generate high quality voxel-by-voxel brain maps.

In addition to the mono and bi-exponential models, other high order diffusion models that have been investigated in clinical gliomas, such as the fractional order calculus model (FROC)

and restricted diffusion model (RDM) [15,38]. Those high-order diffusion models require diffusion weighted images with more b-values and high SNR. The FROC requires b-values up to 4000 s/mm2, and the diffusion coefficient in the model is pre-determined by fitting a mono-exponential model before fitting the entire model [15], which may lead to some errors in parameters. The RDM is insensitive to intracellular diffusion coefficient and is instable to voxel fitting [38], which leads to difficulty in generating parameter maps in the patients with GBM. The diffusion kurtosis model improves the goodness of fit, and is more stable than those high-order diffusion models [15 38]. In addition, the kurtosis model has been investigated in clinical gliomas [29]. Research suggests that mean kurtosis shows better separation of glioma grades than fractional anisotropy and mean diffusivity. Overall, the kurtosis model is convenient to generate voxel maps and provides the potential measurement of non-Gaussian diffusion in GBM.

When considering underlying of tissue morphology and physiology of diffusion parameters, low ADC is considered to correlate with high cellularity. However, co-existence of edema and high vascularity in a single pixel of the tumor can elevate ADC compared to normal white matter and grey matter. To mitigate the influence of perfusion on measured diffusion coefficients, a bi-exponential model that quantifies fast and slow DCs has been investigated. The fast DC derived from the model is found to be significantly higher in high-grade gliomas than in low-grade gliomas [29], which could be due to hyper-vascularization in the high-grade gliomas. One limitation of the bi-exponential model is that the fraction of slow DC component has discordance with microstructure parameters, e.g., the fraction of intra-cellular water. Some investigations suggest that the discordance may result from the restricted cell membrane and cell

size [73,74]. The RDM considers restricted intracellular diffusion and modulations of diffusion gradients into the model [11,38]. To obtain accurate estimations of the apparent cell radius and the extracellular diffusion coefficient derived from the RDM in the GBM and brain normal tissue requires short diffusion times that may be beyond the clinical scanner hardware. The heterogeneous tissue could present even more challenges for the model [38]. The FROC model shows that DC, fractional order and spatial parameter all differentiate high-grade pediatric brain tumors from low-grade ones [15]. In addition, the fractional order has high predictive values for tumor outcomes [15]. There are also some limitations of the FROC model. First, the parameters derived from the model may not differentiate tumor from normal tissue [15]. Another challenge is that parameters are not sensitive enough to generate high contrast maps [15].

Previous research has suggested that the mean kurtosis could serve as the optimal parameter for grading glioma in practice [29]. Zhang et al. investigated the correlation between overall survival (OS) and kurtosis in high grade gliomas, including grade III and grade VI, and found that mean kurtosis of glioma was a significant predictor of OS [66]. Hempel et al. also assessed whether mean kurtosis was prognostic factor in grade II, grade III and grade IV gliomas, and found PFS and OS was significantly better in patients with lower mean kurtosis [75]. However, different grades of gliomas could have specific features, which may contribute to prediction power. In our analysis, we only included grade IV of glioma.

In this study, we found that a high mean kurtosis values pre-RT was significantly correlated with reduced OS. To illustrate the unique contribution of the mean kurtosis, we also tested the Gd-GTV for prediction of survival using the cox model. We found that the Gd-GTV

volume itself did not predict OS, which suggests that the mean kurtosis provides information beyond the enhanced tumor volume. In the Gd-GTV that consists of heterogeneous tumor with mixture of high cellular tumor and edema, the kurtosis values vary from high to low. The region with high kurtosis values may imply an aggressive component in the tumor, which is supported by the observations: 1) a higher grade of gliomas associated with higher mean kurtosis values [29,36] and 2) high mean kurtosis values in GBM associated with inferior survival. The decreased mean kurtosis and the increased DC in the Gd-GTV of GBM after receiving radiation treatment are expected to represent a tumor response to therapy, but not specific enough to predict outcomes. Radiation likely causes cell degeneration and necrosis [76], which may decrease mean kurtosis and increase DC to an extent for some GBMs. In contrast, we observed substantially increased mean kurtosis and decreased DC at the mid-RT in two patients who had rapid tumor growth. Further research could be carried out to investigate pathology associated with mean kurtosis changes.

The DKI model quantifies non-Gaussian water diffusion in heterogeneous tissue and demonstrates the potential to predict OS in GBM patients. However, there are some limitations in the current study. First, we used 11 b-values up to 2500 s/mm^2, which increases acquisition time. Also, the model is sensitive to noise. To overcome the noise influence on model fitting, we applied a 2D Gaussian filter that blurs images. Second, the mean kurtosis decreased while the DC increased in mid treatment, but these changes are not significantly associated with survival. This may be affected by radiation treatment or the small patient size. Third, this is a retrospective analysis with a small sample size. Fourth, pathology correlated to the imaging finding is lacked

in our research. Understanding of the mean kurtosis and DC changes after radiation and relationship to tumor changes are limited. The DKI model needs to be further validated in an independent large cohort of patients in future.

The DKI model demonstrates the potential to predict survival in the patients with GBM. Further development and histopathological validation of the DKI model will warrant its role in clinical management of GBM.

Chapter 4 T2-relaxation-diffusion Correlation Analysis in Glioblastoma

The results described in this chapter were previously described by the author in abstracts for the 2018 ISMRM and 2020 AAPM annual meetings [77,78].

4.1 Introduction

Among the high-order diffusion models, there are very limited research attempting to investigate the T2 and diffusion coefficient (DC) together in GBM. Most researchers investigate T2 and DC separately [9,18,19] . For example, Maier et al [9]investigated brain tumor with bi-exponential diffusion model. This model considers fast and slow diffusion in brain tumor and normal tissue, and separated tumor from other brain tissue in two thirds of patients. In investigation, fractional volume of slow component (Vs) from the model is much lower than experimental result [8] . Another model, called multi-exponential proton spin-spin relaxation model [18,19], uses multi-echoes sequence to investigate multiple T2 decays in tumor and other brain tissue. In their study, white matter and gray matter showed three components and two components T2 decay, separately. Tumor and edema both show bi-exponentiality of relaxation time in investigation [19]. These results suggested that multi-T2 components exist in normal tissue and tumor. However, the long component T2 of tumor was unexpectedly high (>700ms).

Recent studies suggest that a model correlating T2 and DC together could characterize heterogeneous tissue better [17] . The capability of the 2D T2 correlation experiment to improve

the sensitivity has been demonstrated on different tissue types [17,20,21] . This technique used an ill-posed equation with infinite solution [22,23] , which is difficult to directly apply to diffusion curves.

In this study, we simplified the model described in Bernin et al.[16] and applied to two series clinical diffusion weighted images with two different TEs in the GBM patients. We applied the simplified model to the DW images with high b-values to investigate whether any significant differences in the quantified parameters among hypercellular tumors, edema and normal tissue. We also tested parameters with time-to-event analysis model to investigate whether any parameter is significant predictor of progression free survival (PFS) and overall survival (OS). This study was the first step to test the possibility of the application of the model correlating T2 and DC using a widely available diffusion technique on the clinical scanner for GBM.

4.2 Material and Methods

4.2.1 Simplified T2-relaxation-diffusion Correlation

It is an emerging approach to combine multiple contrasts into a single analysis. This approach would allow an exploration of the T2-relaxation-diffusion correlation in brain tumors to better understand tumor physiology than using diffusion or T2-relaxation MRI alone [16] . We assumed diffusion signal can be considered as the sum of slow and fast components:

$$S = S_{f0}\exp(-bD_f)\exp\left(-\frac{TE}{T2_f}\right) + S_{s0}\exp(-bD_s)\exp\left(-\frac{TE}{T2_s}\right) \quad (4.1)$$

where D_f and D_s are fast and slow diffusion coefficients, $T2_f$ and $T2_s$ are associated respective T2 values, S_{f0} and S_{s0} are the amplitudes of respective fast and slow diffusion components, and b is the b-value. V_s is the fraction of the slow diffusion component and calculated as $S_{s0}/(S_{f0}+S_{s0})$.

4.2.2 Patients

Twenty-four patients (median age of 59.5 years, 11 female) with histologically diagnosed GBM were treated with either 60 Gy standard (10 patients) or 75 Gy boosted RT (14 patients) and had diffusion weighted (DW) images pre-RT but after tumor resection or biopsy. The 15 patients had mid-RT scans (week 3) to assess response. The 13 patients had MGMT methylation tests and five in those are positive.

4.2.3 In Vivo MR Imaging

All scans were performed on a 3.0-T scanner (Skyra, Siemens Healthineers) using a 20-channel head coil. Conventional MR images, 2D T2-FLAIR images, and 3D pre- and post-contrast T1-weighted images using a MPRAGE sequence, were acquired. DW images were acquired by a spin-echo echo-planar pulse sequence with diffusion weighting in 3 orthogonal directions and 11 b-values from 0 to 2500 s/mm^2 with an incremental step of 250 s/mm^2. Other acquisition parameters included the parallel imaging factor of 4 (GRAPPA) (to reduce echo spacing and hence geometric distortion), TE/TR=93/9300 ms and 113/9300ms, bandwidth of 1040 Hz/pixel, voxel size of approximately 1.3 x 1.3 x 5.2 mm, 30 slices to cover the whole brain, one average and total scan time of 4.50 min. In addition, DW images with b=3000 s/mm^2 and 4 averages were acquired. All DW images were acquired prior to contrast injection.

4.2.4 Definition of Volume of Interest

Due to anticipated SNR in DW images, we performed this analysis in volumes of interest (VOIs). The challenges in tumor definition of GBM are several fold. Studies of GBM using advanced imaging have shown that solid tumor components can be beyond the contrast enhanced gross tumor volumes[31,47]. Also, the T2 abnormality volume can consist of tumor, edema, and a mixture of the two. However, at high b-values of diffusion imaging, water signals of edema are attenuated much faster than the hyper-cellular tumor. Based upon this hypothesis, in a previous study, a tumor volume was created by combining automated thresholding on the DW images with b=3000 s/mm^2, and then viewed and edited by an attending radiation oncologist who is specialized in brain tumor therapy[47]. The initial tumor volume was created using a threshold of the mean intensity plus 2 standard deviations calculated from a VOI in the normal-appearing tissue most contralateral to the T2-abnormality and performed on the DW images with b=3000 s/mm^2. Also, this tumor volume has shown to be significantly correlated with progression-free survival[47]. Therefore, we used this tumor volume (TV) to characterize T2 and diffusion parameters in this study. Note that this TV is different from the contrast enhanced tumor volume.

To compare the behavior of this model in edema to solid tumor in GBM, an edema volume was created within the T2-abnormality but had at least 1 cm away from both the TV used in this study and the contrast enhanced gross tumor volume. In the cases with tumor recurrence, the edema volume was checked and made sure to have no spatial overlap with the recurrent tumor volume. Also, the VOIs of two large WM fiber bundles were drawn: one in the frontal lobe and another in the Genu of corpus callosum. To compare to GM, cortex regions in the frontal and parietal lobes

were segmented using the fuzzy c-means algorithm on diffusion weighted images with b=0 (T2-weighted images) and ADC maps. To avoid influence of cerebrospinal fluid (CSF), a deep GM structure, the head of caudate nucleus, was carefully chosen. As a total, six VOIs were created, see Figure 4-1.

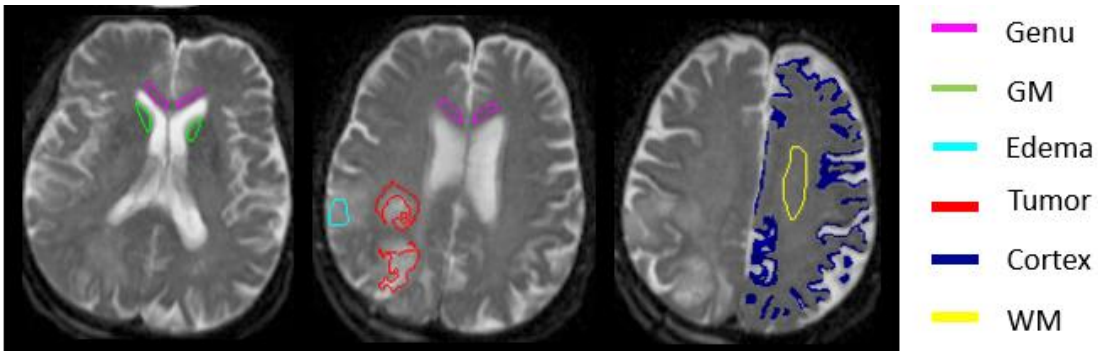

Figure 4-1. Illustration of volumes of interest (VOIs) used in the analysis. Red contours tumor volume on the DW images with b=3000 s/mm2. Magenta, green, cyan, blue and yellow contours represent genu, deep gray matter (head of caudate nucleus), edema, cortex and frontal white matter, respectively.

Prior to the VOI creation, 3D post-contrast T1-weighted images were reformatted into the axial plane with spatial resolution of 1x1x3 mm. All other images acquired within the same session were reformatted to the post-contrast T1-weighted images using coordinates in the DICOM header.

4.2.5 Computation of T2-Relaxation-Diffusion-Correlation Model

T2-relaxation-diffusion-correlation model was implemented using Matlab. The model was fitted to the DW images with 22 b-values using a Simplex algorithm in Matlab. We fitted the model to six parameters of D_f, D_s, $T2_f$, $T2_s$, S_f and S_s. Simplex was initiated randomly in the ranges of the parameters based on prior knowledge of the physiological parameters (S_s: 0-1000, S_f: 0-1000, $T2_s$: 0-100 ms, $T2_f$: 0-100 ms, D_s: 0-0.1 $\mu m^2 ms^{-1}$, D_f: 0-1 $\mu m^2 ms^{-1}$). Fitting was run 100 times, and the results were accepted with the minimum mean squared errors (MSE).

4.2.6 Statistical Analysis

To evaluate changes in the parameters in response to radiation doses after three weeks of RT, Students' t test was used and a p-value less than 0.05 was considered significant. Kaplan-Meier (KM) analysis, univariate and multi-variate Cox proportional hazard model were used to test these parameters for prediction of PFS and p-value of 0.05 was considered significant.

4.3 Results

4.3.1 T2 relaxation diffusion correlation in tissues pre-RT

We mainly focused on $T2_s$, $T2_f$, D_s, D_f and V_s in this investigation. These parameters of six tissue types were summarized in Table 4-1. T2 values of WM and GM were close to a previous research [79] and only 2 WM tissue showed T2 reverse among all tissue types. Table 4-1 summarized p-values results of pure tissue parameters compared to tumor's results. There were significant differences between fast and slow diffusion coefficients and between associated T2 values in tumor, cortex, deep GM, and edema ($p<0.001$). For tumors, cortex, deep GM, and edema, the fast diffusion coefficients (D_f) were associated with elongated T2 values; while for WM including frontal WM and genu, the fast diffusion coefficients were associated with short T2 values. The tumor had D_f significantly greater than WM and deep GM ($p<0.05$) but not cortex and edema, and $T2_f$ significantly greater than all other tissue types ($p<0.05$) except cortex possibly due to the partial volume effect of cerebral spinal fluid (CSF). For the slow compartment, the tumor had significantly greater $T2_s$ than all other tissue types. The D_s in the tumor was not significantly different from all other tissue types. Figure 4-2 showed the T2-

relaxation-diffusion distributions from tumors and normal WM and GM by fitting Eq 4.1. There was a tilting line to separate tumor and other tissues, except cortex. This may be due to CSF contained in cortex. Additionally, we used multivariate logistic regression to test whether we could separate tumor and other tissue types completely. The results were summarized in Table 4-2. From analysis, we found that $T2_s$, $T2_f$ and V_s were significant predictors of tumor (p value=0.02, p value=0.005, p value=0.04, respectively).

In investigation, we also found that $T2_s$ of two diffusion components estimated by the model are significantly different in tumor, genu, cortex and edema (p=0.03, p<0.01, p<0.001, p=0.03).

Table 4-1 Parameters of different pure tissue types with T2-relaxation-diffusion-correlation model analysis.

		$T2_s$ (ms)	$T2_f$ (ms)	Ds/μm^2/ms	Df/ μm^2/ms	V_s
Tumor	Mean ±SEM	148.6±18.2	227.9±24.2	0.31±0.034	2.02±0.20	0.44±0.045
Frontal WM	Mean ±SEM	114.9±4.8	110.1±6.0	0.19±0.020	1.43±0.046	0. 36±0. 033
	P value	No Sig	p<0.001	p<0.01	p=0.012	No Sig
Genu	mean ±SEM	103.3±2.9	81.0±5.2	0.15±0.024	1.65±0.073	0. 28±0. 027
	P value	p=0.028	p<0.001	p<0.01	No Sig	p=0.011
Deep GM	mean ±SEM	80.3±5.2	100.5±11.3	0.26±0.028	1.59±0.098	0. 44±0. 041
	P value	p<0.01	p<0.01	No Sig	No Sig	No Sig
Cortex	mean ±SEM	73.3±2.9	256.7±40.7	0.51±0.012	2.40±0.072	0. 44±0. 041
	P value	p<0.01	No Sig	p<0.001	No Sig	No Sig
Edema	mean ± SEM	104.0±14.4	162.6±19.3	0.36±0.048	1.83±0.10	0.39±0. 053
	P value	No Sig	No Sig	No Sig	No Sig	No Sig

Note: All p –values are acquired from comparison of tumor parameters to corresponding tissue parameters. No Sig represents no significance found.

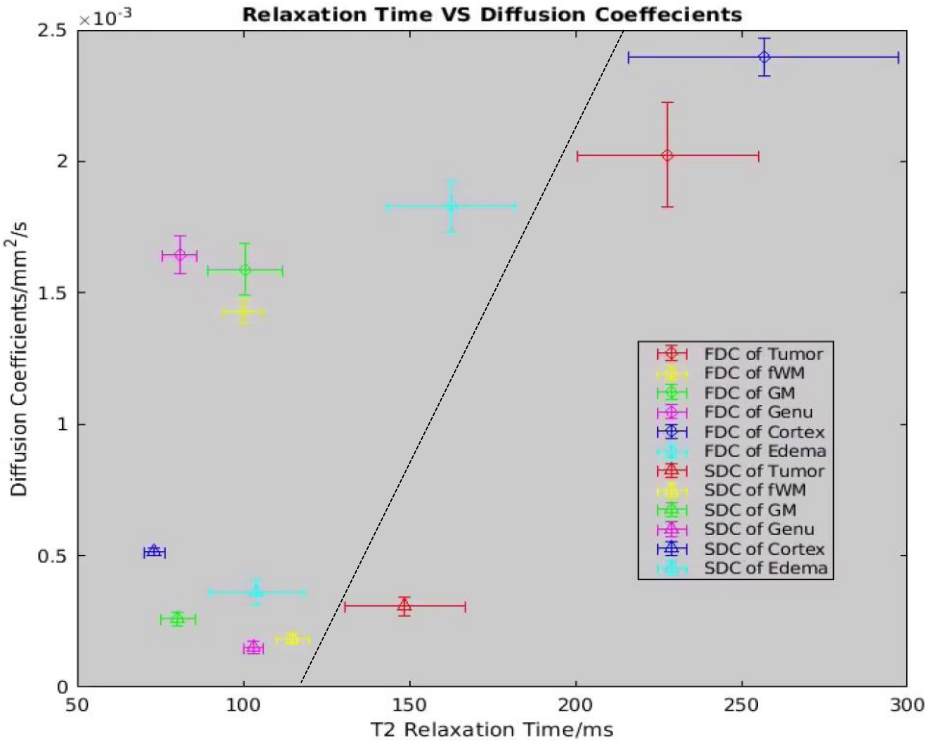

Figure 4-2 T2-relaxation-diffusion distributions in 6 kinds of tissue types. Horizontal error bars are the SEM of T2-relaxation time and vertical error bars are the SEM of diffusion coefficients.

Table 4-2 Multi-variate logistic regression of the parameters from the T2-relaxation diffusion correlation model to predict tumor

	$T2_s$	$T2_f$	V_s
Coefficient	0.007	0.016	5.56
P value	0.02	0.005	0.04

4.3.2 Estimated parameters of pre-RT and mid-RT in two patient groups

We investigated pre/mid-RT TV in two patient groups who received different radiation doses and summarized results in Table 4-3. In boosted group, $T2_s$ at mid-RT increased significantly 326%±366% (p=0.023) compared to pre-RT. The large increase in $T2_s$ of the boosted group may suggest that higher doses could cause necrosis and increased fluid content in the tumor. In standard group, $T2_s$ increased 19%±39%, but not significant. Changes in other parameters of two groups were also not significant.

Table 4-3 Parameters of pre-mid-RT standard and boosted group with T2-relaxation-diffusion correlation model analysis

	$T2_s$ (ms) (mean ± SEM)	$T2_f$ (ms) (mean ± SEM)	D_s/ μm^2/ms (mean ± SEM)	D_f/ μm^2/ms (mean ± SEM)	V_s (mean ± SEM)
Pre-RT standard	174.1±31.7	266.2±45.7	0.35±0.02	2.15±0.12	0. 43±0.05
Mid-RT standard	187.8±33.7	145.3±21.2	0.31±0.04	2.00±0.10	0. 32±0. 03
Pre-RT boosted	105.6±8.4	101.9±6.4	0.24±0.03	1.59±0.07	0. 41±0. 04
Mid-RT boosted	383.8±92.7	167.7±39.5	0.28±0.03	2.02±0.14	0. 26±0. 13

Changes of $T2_s$ were significantly different between the two groups (p=0.032). Changes in D_s, D_f and $T2_f$ didn't show significant differences between two groups, but these three in boosted group all increased more than in standard group. In this study, we found there were large differences between parameters pre-RT in the two groups, especially in two T2 values. Thus, we

investigated Gd-GTV pre-RT to assess whether there were significant differences in these two groups additionally. The results are summarized in Table 4-4. We found significant differences between the two groups in Gd-GTV volume (p=0.046). The patients who were in the boosted group could be selected with smaller tumor volumes or more extent of surgery, but the percentage changes in $T2_s$, $T2_f$ and DCs between the two groups were unlikely due to the bias of patient selection in the clinical trial with radiation boosting.

Table 4-4 GTV pre-RT volumes of standard and boosted group

	Volume/mm3 (mean ± SEM)	Median volume/mm^3	Minimum volume/mm^3	Maximum volume/mm^3
standard group	35103.1±5577.7	32085.7	20973.0	62501.7
boosted group	20435.5±3096.4	19722	5718.2	36610.0

4.3.3 Parameters correlate with PFS

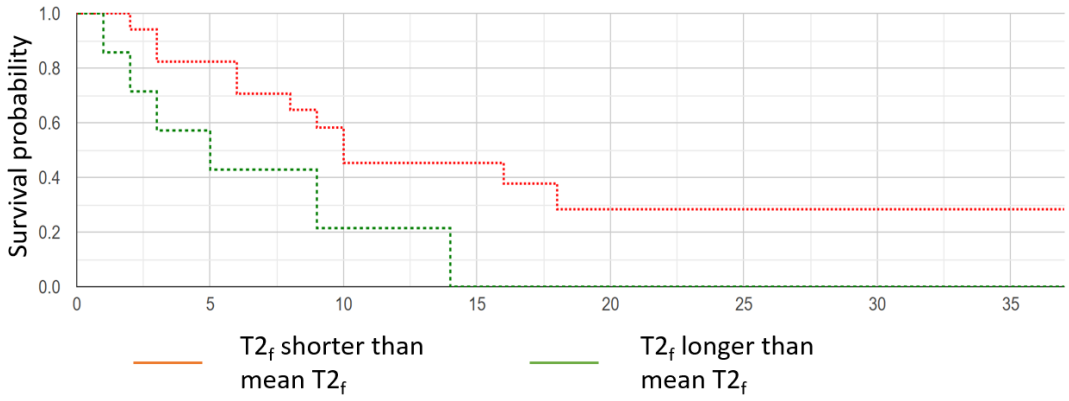

Figure 4-3 Kaplan-Meier Curves of PFS. Two groups were defined by greater (green) or shorter (red) than the mean fast T2 value tumor (p=0.05)

Long $T2_f$ in the pre-RT TV was significantly associated with inferior PFS by Kaplan-Meier (KM) analysis (p=0.05), suggesting long $T2_f$ could be associated with severe disease. From the previous result, $T2_f$ of TV showed larger difference with other normal tissue than $T2_s$. This may be the reason that $T2_f$ showed significant by KM analysis while $T2_s$ not.

In addition to KM analysis, we analyzed the data with Cox proportional hazard model. Univariate Cox model analysis showed that V_s at mid-RT in the tumor was significantly associated with reduced PFS (HR=3.6, p=0.02; Table 4-5), but not the values measured at pre-RT (p value =0.45). In addition to V_s, we classified the other four parameters into two classes by their averages and tested these classes with the univariate cox model. We also found that $T2_f$ pre-RT was significantly associated with reduced PFS (HR=2.83, p=0.05; Table 4-5.), but not $T2_f$ mid-RT (p=0.41). Univariate Cox model analysis of clinical prognostic factors for prediction of PFS were listed in Table 4-5.

We further addressed the question whether V_s and $T2_f$ added any values than clinical prognostic factors, such as age, dose and extent of surgery (EOR), for prediction of PFS. After adjusting these clinical factors, the Vs mid-RT was a significant predictor of PFS (HR=9.9, p=0.02; Table 4-6), and the T2f pre-RT was also a significant predictor of inferior PFS (HR=2.84, p=0.05; Table 4-7).

Table 4-5 Univariate cox proportional model analysis in V_s mid-RT, $T2_f$ pre-RT and clinical factors with PFS

	Hazard ratio (HR)	p-value	95% CI
Vs mid-RT	3.57	0.02*	[1.24, 10.26]
T2f pre-RT	2.83	0.05*	[1.00, 8.09]
age	1.53	0.21	[0.79, 2.94]
MGMT	0.14	0.07	[0.02, 1.17]
EOR	1.43	0.39	[0.63, 3.21]

Table 4-6 Multivariate cox proportional model analysis in Vs mid-RT and clinical factors with PFS.

	Hazard ratio (HR)	p-value	95% CI
Vs	13.24	0.02*	[1.66, 105.43]
age	3.46	0.11	[0.76, 15.67]
MGMT	0.16	0.21	[0.01, 2.84]
EOR	1.87	0.51	[0.29, 11.95]

Table 4-7 Multivariate cox proportional model analysis in T2f pre-RT and clinical factors with PFS.

	Hazard ratio (HR)	p-value	95% CI
$T2_f$ pre-RT	2.84	0.05*	[1.00, 8.15]
age	1.36	0.29	[0.77, 2.42]

4.4 Discussion

In this study, we simplified the model of Bernin et al. [16] to fit the DW images and characterize diffusion properties of the hypercellular tumor in the patients with GBM. In investigation, we found that modeling T2 and DC together helps differentiate tumor from edema and normal tissue. Parameters estimated from T2-relaxation-diffusion model, such as $T2_f$ and V_s, correlated with PFS and showed the potential to predict survival. ADC that ignores multicomponent of heterogeneous diffusion in brain tissue may fail to differentiate tumor and other tissue [4-7,39]. The parameters from the T2-relaxation-diffusion model could identify the TV better than a single metric. The V_s and $T2_f$ may add value to clinical factors and help predict progression better. The T2-relaxation-diffusion model has a great promise to aid into conventional MRI for GBM diagnosis, image-guide therapy, and response assessment. Further validation with histopathology will warrant the role of the model in the clinical management of GBM.

Many diffusion models have been investigated in gliomas. An apparent diffusion coefficient (ADC) quantified from conventional DW images with b-values between 0 and 1000 s/mm^2 using a mono-exponential decay is the commonly reported parameter in literature. Previous studies have suggested that a low ADC was associated with a decrease in survival for patients with gliomas [30,69-72]. One limitation of mono-exponential model is that there are large deviations of fitted curves from the diffusion weighted signal when b-values are greater than 1500 s/mm^2. Another problem is that one parameter is difficult to describe the complex microstructure effects on water diffusion. To deal with the deviation of diffusion weighted signals from the mono-

exponential function, a bi-exponential model with fast and slow diffusion components is propose [8]. In the initial interpretation of the bi-exponential model, fast and slow diffusion coefficients are considered from respective extra- and intra-cellular water compartments, but the estimated faction of the intra-cellular water in the tissue from the bi-exponential model cannot be matched with the other measures [9]. Previous research usually measured T2 and DC separately in brain tumor [9,18,19] , but T2 and DC are correlated. Different TE will influence DC values in mono- and bi-exponential models. TE that is long enough will lead to elimination of intracellular diffusion signal and DC values derived from the two models should be the value of extracellular DC. A very short TE will lead to detection of intracellular DC component in the two models. Also, Multiple T2 components will influence intracellular fraction volume of signal in bi-exponential model, which could be explained by that different DCs have different T2 values. Multiple T2 components in human brain tissue has been investigated [18,19]. Schad et al. implemented multiple echoes to investigate multicomponent T2 in brain tumor [19]. They demonstrated that two components T2 of tumor, edema and CSF were observed, but WM and GM followed mono-exponential T2 decay. Other researchers presented different result and demonstrated WM and GM have at least two components of T2 [18] . They showed WM has three T2 components with a minor component less than 11% (T2 between 10 and 55ms) and GM has two component T2 close to 100 ms. After ignoring the minor part, it is reasonable that the T2-relaxation-diffusion model considers two components of diffusion curves and combines T2 and DC together, which help characterize T2 values and DCs better.

When considering underlying of tissue morphology and physiology of diffusion parameters, low ADC is considered to correlate with high cellularity. However, co-existence of

edema and high vascularity in a single pixel of the tumor can elevate ADC compared to normal white matter and grey matter. To mitigate the influence of perfusion on measured diffusion coefficients, a bi-exponential model that quantifies fast and slow DCs has been investigated. The fast DC derived from the model is found to be significantly higher in high-grade gliomas than in low-grade gliomas [29], which could be due to hyper-vascularization in the high-grade gliomas. Multiple T2 components correlated with multiple DCs in a VOI could lead to factorized signal amplitude of two components, thus resulting in un-expected low intracellular fraction. Maier et al. [9] discussed in their research that intracellular fraction of tumor (0.24±0.10) derived from bi-exponential DC model is much lower than previous experimental result [8]. Our V_s derived from the T2-relaxation-diffusion model is 0.43±0.11 (mean ± SD). Though V_s is still lower than experimental result, it is much higher than result of Maier et al [9].

In our current study, T2 values of two diffusion components estimated by the model are significantly different in tumor, genu, cortex and edema. GBM is heterogeneous tumor with mixture of high cellular tumor, normal tissue and edema, for which diffusion coefficients vary from low to high, resulting in inconsistent and often elevated apparent diffusion coefficients (ADCs) when using conventional b-value (1000 s/mm^2 or lower) [4-7]. That two components have two different T2 values suggests that using different TEs for ADC measurement in GBM could lead to different ADC values. One single metric may not be accurate enough to identify features of the tumor.

$T2_f$, D_s and D_f increased in boosted group after radiation therapy but decreased in standard group. $T2_s$ increased in both groups. Our previous results indicate that tumor tends to have higher

T2 values and DCs, but researchers have suggested boosted group has better outcome in other in other investigation [49] . There could be multi-factors that contribute to the increase of parameters. Tumor tends to have larger T2 values and DCs, but this elevation in mid-RT tumor could also result from tissue response after radiation, and we will explain it from several points. Previous research has demonstrated that there could be ADC elevation after radiation dose and this increase may result from necrosis [76] . Water content *in vivo* has almost positive correlation with T2 [80] , which helps explain that elevation of T2 could also result from necrosis. Also, cell permeability and tissue inflammation could increase DCs after radiation. In our investigation, V_s in boosted group also decreased. V_s is slow diffusion component and may represent the extent that water is restricted in tissue. The decrease of V_s may indicate the water is less restricted in tissue, which may be due to cell degeneration after radiation. Thus, we think that the elevation of T2 and DC is mainly due to response after radiation, and it is very likely to have this increase. Further validation could be carried out to investigate whether boosted radiation dose will lead to more necrosis than standard dose.

In our result, larger pre-RT $T2_f$ was significantly correlated with lower PFS rate in KM analysis and cox proportional hazard model, which imply T2f may have the potential to predict PFS. Our TV was created using a threshold to the T2-abnormality and performed on the DW images with b=3000 s/mm^2, which exclude the edema-dominated region. From the comparison of the pre-defined TV and normal tissues, the solid tumor has larger $T2_f$ than any other tissues. This could be one reason that why $T2_f$ has the potential. Also, we found $T2_f$ and D_f showed positive correlation in investigation, which may indicate D_f could be related with progression. Further

research could be carried out to investigate whether D_f and $T2_f$ are both significantly correlated with progression in large patient number.

To further investigate the behavior of the T2-relaxation-diffusion correlation model, we tested additional five patients with three distinct TE (TE=70ms, 90ms and 110ms, respectively) and fitted the model. Every patient was diagnosed histologically diagnosed GBM. we compared the averages of parameters between the three-TE patients and the two-TE scanned patients in TV. From the analysis, we didn't find large differences (< 10% in all five parameters) between the three-TE derived parameters with the two-TE derived parameters in the TV.

The T2-relaxation-diffusion model modeled DC and T2 together and demonstrated the potential to predict PSF of GBM patients. However, current study has some limitations. First, we used 2 TE and 11 b-values in analysis, which will increase acquisition time in scans. The model has six parameters totally, but not very stable with these acquisition data. $T2_s$ was estimated larger than 600ms sometimes in small VOI with minimum MSE, and parameters need to be selected within physiological range manually. Multi-TE acquisition may help stabilize the model and need to be further validated in the future. Second, our sample size is not large with only 24 pre-RT and 15 mid-RT patients. In our investigation, mid-RT $T2_s$ was significantly different from pre-RT $T2_s$ in both groups but was not a significant predictor in cox model. This may result from the small sample size. The T2-relaxation-diffusion model needs to be further validated in an independent large cohort of patients in future.

Chapter 5 Analysis of Diffusion and Microstructure Properties in Brain Tumors Using a Random Walk with Barriers Model

The results described in this chapter were previously described by the author in an abstract for the 2021 AAPM annual meeting [81].

5.1 Introduction

High-order diffusion models have been explored in clinical gliomas to differentiate tumor grade and assess therapy response [8,9,15,32,36,39-42]. Among the high-order diffusion models, a few of models attempt to quantify microstructures in tumors from macroscopic diffusion imaging[14,24,43]. Microstructure alterations caused by pathological changes could potentially be captured by studying water diffusion. A model, called random walk with barriers model (RWBM), considers that water diffusion in microstructural tissue is restricted by cellular structure membranes and thereby a measurement (diffusion) time during which water molecules travel through cell membranes and structures affects the measured water diffusion coefficient [27]. The RWBM could analyze these effects on diffusion to reveal microstructural properties from macroscopic imaging characteristics within heterogeneous brain tumors.

Recent studies [24,25] investigating the RWBM in prostate showed that lumen length and membrane permeability agreed with known values from tissue histology and membrane biophysics. This study also extended the investigation into prostate cancer and suggested that the RWBM may be a powerful biophysical model to provide information on prostate cancer grading.

However, there are very limited efforts in investigating microstructures in brain tumors using the RWBM.

In this study, we applied the model described by Novikov et al. [27] to diffusion weighted images in the patients with brain metastases and GBM. A prototype diffusion gradient sequence that is able to crate oscillating gradient waveforms was used to achieve short diffusion times in acquired diffusion weighted (DW) images. We applied the RWBM to the DW images to investigate whether any derived parameter reveal the features of the brain tumors. Another model, called three-distance diffusion model, was also investigated whether this model could reveal biophysical characteristics and was compared with the RWBM. The requirements of DW image collections to apply these two models on gradient hardware of a clinical scanner were also investigated. This study was the first step to test the potential of the application of the models quantifying microstructure parameters for brain tumors.

5.2 Material and Methods

5.2.1 RWBM

In the RWBM, researchers considered that restrictions to diffusion could be represented by extended membranes [27]. Novikov et al. [27]assumed that extended membranes could introduce significant long-range correlations between the cell structure and water diffusion, which is different from those due to the short-range disorder.

In the RWBM, there are three distinct regimes of time-dependent diffusion coefficients separated by short and long-time limits [27].

In the short-time limit, the time-dependent diffusion coefficient is given by:

$$D(t) = D_0\left[1 - \frac{S}{Vd}\left(\frac{4\sqrt{D_0 t}}{3\sqrt{\pi}} - \kappa t\right)\right] \quad (5.1)$$

where D_0 is an unrestricted diffusion coefficient, S/V is a surface area to volume ratio of the cell or the structure of restricting water diffusion, d is the dimension of the structure of interest, and κ is the permeability of the cell or structure membrane. The range of diffusion times (t_D) over which we could apply the S/V limit (Eq. 1) is that $t_D \ll$ cell size^2/(2dD_0) [2]. In analysis, we first estimated cell size and D_0 with two measurements with short diffusion times and calculated $t_{estimation}$= cell size^2/(2dD_0), ignoring the "κt" term in the Eq.1. Whether the measured data satisfied the short time limit was evaluated iteratively. First, the estimated parameter $t_{estimation}$ was used to test whether a loose threshold was met: $\sqrt{\text{diffusion time}/t_{estimation}} < 0.5$. If the diffusion satisfied the threshold, we would estimate cell size, D0 and κ with three diffusion measurements from the Eq. 1 and test whether $t_{estimation}$ satisfy the threshold again. The results with the "κt" term would be accepted if the threshold were satisfied.

In the Long-time limit, the time-dependent diffusion coefficient behaves as:

$$D(t) = D_{inf} + A * t^{-\upsilon}, t \to inf \quad (5.2)$$

where D_{inf} is a bulk diffusion coefficient in the long-time limit, A is the associated strength of the structure disorder, and υ is a dynamical exponent related with underlying structures. When the exponent $\upsilon = 1$, this model is considered as a hyper-uniform disorder. The hyper-uniform disorder is a 1/t tail if a tissue compartment corresponds to fully restricting cell walls, and it could describe diffusion signals from tumors [11,14,43,82,83]. When the exponent $\upsilon = \frac{1}{2}$, this model is

considered in an extended disorder. This disorder geometry was approximately described that cell membrane is highly permeable. $\upsilon = \frac{1}{2}$ applies if the cell walls are sufficiently permeable. In our analysis, we first estimated a long-limit diffusion time threshold ($t_r = \frac{v^2}{s^2 d} / (\frac{1}{D_{inf}} - \frac{1}{D_0})$). We then fitted both hyper-uniform disorder and extended disorder equations to the data and checked relations between t_r and diffusion time to determine which disorder assumption was satisfied. We would consider the hyper-uniform disorder if t_r < diffusion time, and the extended disorder if t_r > diffusion time.

The equations of the RWBM were fitted to the mean, perpendicular and parallel diffusion coefficients that were calculated from DW images with three diffusion times to derive the D_0, S/V, κ, and D_{inf}. Cell diameter was estimated by 2d*V/S.

5.2.2 Three-distance diffusion model

There is another model considers restricted diffusion governed by the interplay of three lengths: diffusion length (l_D), length of structure (l_s) and dephasing length (l_g) [37].

In the diffusion length (l_D), we calculated $l_D = \sqrt{D_0 * t}$, where D_0 is the unrestricted diffusion coefficient. Within the l_D regime, diffusion is unrestricted, free diffusion. The length of structure (l_s) is considered as the cell size of tissue. In the ls regime, the water molecules have traveled the cell length a few times before the magnetization dephasing. In the dephasing length ($l_g = (D_0/\gamma g)^{1/3}$, where γ is the gyromagnetic constant and g is the diffusion gradient

amplitude, water spins that are far away from the cell membrane have completely de-phased, but molecules within length l_g of the membrane cells were dephasing.

We simply called this model the three-distance diffusion model. This model allows to estimate the structure length l_s, which will be compared with the ones estimated by the RWBM.

In the l_D regime, the diffusion signal is formulated as:

$$S/S_0 = e^{-b*D_0} = e^{-\frac{2}{3}\left(\frac{l_D}{l_g}\right)^6} \tag{5.3}$$

where S is the amplitude of diffusion signal, S_0 is the amplitude of diffusion signal at 0 b-value, and D_0 is an unrestricted diffusion coefficient. After a logarithm to diffusion signals, the signals decay linearly with $\left(\frac{l_D}{l_g}\right)^6$.

In the l_s regime, the diffusion signal is formulated as:

$$S/S_0 = e^{-\frac{1}{60}\left(\frac{l_D}{l_g}\right)^2\left(\frac{l_s}{l_g}\right)^4} \tag{5.4}$$

where the logarithmic diffusion signal is decay linearly with $\left(\frac{l_D}{l_g}\right)^2\left(\frac{l_s}{l_g}\right)^4$. The ls could be estimated through Eq. 4 if measured molecule diffusions are in this regime.

And in the l_g regime, the diffusion signal is formulated as:

$$S/S_0 = c\frac{l_g}{l_s}e^{-a1\left(\frac{l_D}{l_g}\right)^2} \tag{5.5}$$

where c and a1 are geometry related constants. The analytical formulae of c and a1 are provided by the previous work [84]. Again, the diffusion signals multiplied with $\frac{l_g}{l_s}$ decay linearly with

$\left(\frac{l_D}{l_g}\right)^2$ after logarithm. The l_s could be also estimated through Eq. 5 if most molecules are diffused in this regime.

With the D_0 estimated from the RWBM, the equations of the three-distance diffusion model were fitted to the mean, perpendicular and parallel diffusion signals at PGSE to derive the l_s.

5.2.3 Patients

Eight patients with brain metastases and two patients with glioblastomas were included in this study that has been approved by an institutional review board. All patients had MRI scans post-surgery but prior to chemoradiation therapy.

5.2.4 In Vivo MR Imaging

All scans were performed on a 3.0-T scanner (Siemens Healthineers) using a 20-channel head coil. Conventional MR images, 2D T2-FLAIR images, and 3D pre-contrast T1-weighted images using a MPRAGE sequence, were acquired. DW images were acquired in three different diffusion time using a prototype sequence of pulsed gradient spin echo (PGSE) and oscillating gradient spin echo (OGSE) at frequency 30Hz (OGSE30) and 50Hz (OGSE50). DW images were acquired in 6 diffusion directions with 8 b-values (0 to 2600 s/mm^2) for PGSE, 6 b-values (0 to 1300 s/mm^2) for OGSE30 and 5 b-values (0 to 500 s/mm^2) for OGSE50. Other acquisition parameters included the parallel imaging factor of 4 (GRAPPA) (to reduce echo spacing and hence geometric distortion), TE/TR=102/3300 ms, bandwidth of 1040 Hz/pixel, voxel size of approximately 2 x 2 x 7.15 mm, 16 slices to cover the major tumor volumes.

5.2.5 Computation of Diffusion Models

The RWBM were implemented by our software developer using in-house Functional Analysis Tools (imFIAT). The three-distance diffusion model was analyzed in Excel. The gadolinium enhancement gross tumor volumes (Gd-GTV) on post-Gd T1 weighted images were delineated by radiation oncologists who treated the patients. Surgical cavities were removed from the Gd-GTV. The delineated GTV-Gd of each tumor, if > 1 cm^3, was classified to smaller volumes using DW image intensities and fuzzy c-means. Also, the volume of interests (VOIs) of white matter (WM) fiber bundles was drawn in the frontal lobe.

The RWBM was applied to three set of DW images (PGSE, OGSE30 and OGSE50) with different diffusion times in the GTV-Gd and WM to yield five parameters using average, perpendicular and parallel diffusivities: cell diameter, D_0, D_{inf}, and κ.The three-distance diffusion model was applied to PGSE images in the GTV-Gd and WM to derive ls in the three diffusivities, similar to the RWBM. The ls with the minimum mean squared error (MSE) was accepted.

Previous research [38,55] have suggested that fractional anisotropy (FA) of infiltrated tumor largely decreased. Therefore, it is reasonable to omit anisotropic diffusion in brain tumors and investigated in the mean diffusion coefficients of three directions. To study how the RWBM behaves in the brain tumor, we investigated the perpendicular directions additionally.

In large WM fiber bundle mainly consisting of axon, the cylinder shape assumption was used. We investigated the two models using diffusion coefficients in perpendicular and parallel directions to study microstructural properties of axon in parallel and perpendicular directions.

5.2.6 Statistical analysis

To evaluate whether the parameters fitted from the RWBM showed different results in the average and perpendicular directions in tumor, Student's t-test was used and a p-value of 0.05 was considered significant.

5.3 Results

5.3.1 RWBM

The microstructural parameters in the Gd-GTVs of the 10 patients were calculated using average and perpendicular diffusivities using the RWBM and were compared. An example of time dependent diffusion coefficients in a metastatic lesion is shown in Figure 1. In this example, the short-time limit of RWBM yielded a free diffusion coefficient D_0 of 2.5 $\mu m^2/ms$, and the long-time limit resulted in a bulk diffusion coefficient D_{inf} of 0.52 $\mu m^2/ms$. Note that diffusion coefficients exhibit systematic dependency on diffusion times. Similarly, we investigated the WM using the RWBM. All data were summarized in Table 5-1 and Table 5-2.

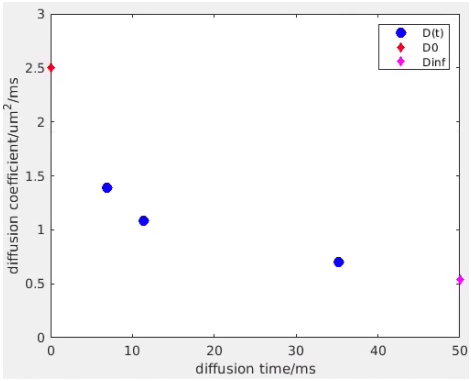

Figure 5-1 Scatter plot of time-dependent diffusion coefficients from one tumor volume. Blue dots are diffusion coefficients calculated from PG, OG30 and OG50; red diamond is D0 calculated from the RWBM at a short-time limit; magenta diamond is D_{inf} calculated from the RWBM at a long-time limit.

Table 5-1 Parameters in Gd-GTV derived by the RWBM

Parameters	Average Results (mean ± SD)	Perpendicular Results (mean ± SD)
D0 ($\mu m^2/ms$)	2.20±0.70	2.02±0.61
Cell diameter (μm)	16.5±4.20	18.23±3.90
κ ($\mu m/ms$)	0.053±0.009	0.067±0.011
D_{inf} ($\mu m^2/ms$)	0.60±0.14	0.75±0.18

Table 5-2 Parameters in WM derived by the RWBM

Parameters	Perpendicular Results (mean ± SD)	Parallel Results (mean ± SD)
D0 ($\mu m^2/ms$)	0.87±0.09	1.87±0.15
Cell diameter (μm)	12.60±0.86	19.78±1.60
κ ($\mu m/ms$)	0.061±0.011	0.08±0.005
D_{inf} ($\mu m^2/ms$)	0.40±0.04	0.85±0.033

The mean and perpendicular diffusivities in all Gd-GTV clusters of brain tumors satisfied the criteria for the short-time limit with two diffusion measurements and the hyper-uniform disorder of the long-time limit. Table 5-1 showed the microstructural parameters in the GTV clusters estimated from mean and perpendicular diffusion coefficients to test whether there were anisotropic diffusion effects on the parameter estimation in brain tumors. There were no

significant differences between the two, suggesting there was no large enough anisotropic diffusion in the GTV-Gd to affect the estimated parameters. Also, in the small number of patients, the significant parameter differences between brain metastases and GBM were not seen. The cell size estimated by average diffusivities was closed to a previous study [59], which suggested that our current diffusion time is short enough to estimate the cell size of brain tumors.

The perpendicular diffusivities in all WM VOIs satisfied the criteria for the short-time limit using first two diffusion time measurements and the hyper-uniform disorder of the long-time limit. Approximately 20% of WM VOIs satisfied the criteria for the short-time limit using three diffusion time measurements and the hyper-uniform disorders in parallel diffusivities, and others satisfied the two diffusion data measurement and the hyper-uniform disorders in parallel diffusivity. Table 5-2 showed the microstructures in white matter. The perpendicular and parallel diffusivities yielded significantly different D0, κ, and D_{inf} values ($p < 0.001$), which could be related to directional axon and myelin sheets structures and properties. The cell dimensions estimated by the perpendicular and parallel diffusivities were related to axon diameter and length, respectively. Note the axon diameter is much larger than expected (~2um), which suggest that diffusion time that can be achieved on a clinical scanner is not short enough for such estimation.

5.3.2 Three-distance diffusion model

We also investigated diffusion data using the three-distance diffusion model. In brain metastatic tumors, we investigated in average diffusion coefficients from three directions due to low anisotropy diffusion. In glioblastoma, we investigated in perpendicular diffusivities due to

residual anisotropy diffusion, which is possibly due to mixed tumor cells with normal tissue. The ls values of all tumor clusters were estimated though Eq. 4. We calculated the percentage of differences (difference%) between ls and cell size derived from the RWBM and didn't find significant differences between the two. The average difference% is less than 20%. All results are summarized in Table 5-3.

Table 5-3 l_s values in tumor estimated by the three-distance model and compared to ones by the RWBM

l_s in Brain metastases (μm)	Difference%	l_s in glioblastoma (μm)	Difference%
17.16±2.39	19.21±14.43	16.29±3.05	15.72±17.71

Difference%: percentage difference of estimated cell dimensions between the three-distance model and the RWBM

Additionally, we investigated frontal WM (fWM), right corpus callosum (RCC), and splenium using the three-distance diffusion model in two GBM patients. Perpendicular and parallel diffusivities were investigated due to the high anisotropy in WM fiber bundle. The values of ls were compared with the cell size estimates derived from the RWBM. The ls values of fWM and RCC estimated using the perpendicular and parallel diffusivities were close to the corresponding estimates from the RWBM, while splenium had larger differences. All results are summarized in Table 5-4.

Table 5-4 l_s results and difference% with cell size derived from RWBM in fWM, RCC and splenium

	l_s in perpendicular diffusivity (μm)	Difference%	l_s in parallel diffusivity (μm)	Difference%
fWM	11.89±0.10	1.50±0.47	17.19±0.016	4.80±3.04

RCC	12.94±0.22	17.86±6.12	21.12±0.28	4.11±2.20
splenium	11.24±1.09	27.96±24.78	20.40±0.015	36.48±11.41

Difference%: percentage difference of estimated cell dimensions between the three-distance model and the RWBM

5.4 Discussion

In this study, we tested the two model of [27] [37]to fit the DW images with PGSE and two OGSE and characterize microstructure and diffusion properties of the brain tumors in the patients. In analysis of the RWBM, we found that the four parameters (D_0, cell diameter, κ and D_{inf}) in the brain tumors did not show the anisotropic differences in the averaged and perpendicular diffusivities, and the estimated tumor diameter is close to what is reported by a previous research [59]. The l_s values estimated from the averaged and perpendicular diffusivities of the brain tumors using the three-distance diffusion model were close to the RWBM cell size. The four parameters estimated in the WM using the RWBM were substantially and significantly different in the perpendicular and parallel diffusivities, but the estimated axon diameter and length had substantially differences with literature [85,86], although the values of fWM and RCC showed agreement between the two models. The RWBM has a great promise to aid into conventional MRI for diagnosis, image-guide therapy and response assessment of brain tumors. Further validation with histopathology will warrant the role of the RWBM in the clinical management.

In the current study, the tumor cell size in GBM estimated from the RWBM in the averaged diffusivity was 16.5±4.20 μm. A pathological study in GBM shows that the radius of

GBM cells can be as large as 20 μm with a mean of 10 μm and a standard deviation of 11 μm (ref). The size of the estimated cell diameter in our model is close to the reported cell size. We also estimated the diffusion time to probe the GBM cell size was around 12 ms, which was pretty close to our current diffusion time in OGSE30 (13.5 ms). We also measured another diffusion signal with lower diffusion time (6.9 ms) and this could be the reason why our estimated cell size showed agreement with previous pathological results.

In the investigation, we also compared the RWBM derived cell size with the l_s. In most tumor clusters, the percentage of differences between l_s and cell size usually are not high (~10%) estimated from the averaged and perpendicular diffusivities but were much higher (~30%) in some clusters that contained either fluid or high cellularity contents. We believed that this discrepancy could be mainly due to that we directly fitted the three-distance diffusion model with D0 derived from the RWBM. The D_0 from the RWBM was calculated through PGSE and OGSE, which could have differences with D_0 that we should use in the three-distance diffusion model. With the assumption of D_0=3 μm^2/ms, the diffusion gradient that is required to explore a 20-μm cell diameter using the three-distance diffusion model was estimated as $1.7*10^{-7}$ T/μm, which is below the maximum gradient can be achieved on our clinical scanner ($4.3*10^{-6}$ T/ μm). This may explain why the l_s values of tumor are close to the RWBM derived cell size. The cell size could be estimated using both models with the diffusion data acquired on our clinical scanner except that the RWBM requires a sequence to achieve short diffusion times, e, g., an oscillating diffusion gradient sequence.

The RWBM derived WM cell dimension using the parallel diffusivity is 19.78±1.60 μm, which could be the averaged axon myelinated segment length plus other cell structures. but previous research suggested that the axon length should be over 100 μm [85,86], which is substantially larger than our results. It is most likely that the diffusion times that are not long enough cause the underestimation of the axon length. The theoretical diffusion time for estimating the axon length could be as long as 400ms with an assumption of D_0=3.0 μm^2/ms, which is 10-fold of our current diffusion time. We could not prolong the current TE to accommodate the long diffusion time requirement, because a long TE (> 200 ms) would result in substantial T2 loss in WM. The WM cell diameter estimated form perpendicular diffusivity is 12.60±0.86 μm, which substantially larger than we expected (~2 μm). This overestimation implies that the diffusion time that can be achieved on a clinical scanner is not short enough for such estimation. With D_0=3.0 μm^2/ms, the theoretical diffusion time to estimate the axon diameter should less than 0.3 ms, which is far beyond the OGSE that we could apply in the scanner currently.

The three-distance diffusion model may not provide accurate estimations for axon dimensions from perpendicular and parallel diffusivities in our current investigation, either. The estimated ls is substantially larger using perpendicular diffusivities, but smaller using parallel diffusivities. To probe the very small axon diameter, a high diffusion gradient with approximately $1*10^{-5}$ T/μm should be applied, which is beyond the maximum gradient ($4.3*10^{-6}$ T/μm) in our current clinical scanner. An estimated low diffusion gradient ($6*10^{-9}$ T/μm) that needs to be accompanied by a very long TE (> 200 ms) should be applied if we use this model to

estimate axon length. This very long TE would result in T2 loss of WM, which is not fitted in brain scanning. Another problem is that we estimated the diameter directly with D_0 derived from the RWBM, which may not be the D_0 that we should use to calculate l_D.

The RWBM demonstrated the prognostic potential and the opportunity to reveal features in brain tumors. However, the current study has a few limitations. First, our sample size is not large, with only 10 patients. The small number of patients causes a potential bias. The RWBM needs to be further validated in an independent large cohort of patients in future. Second, we satisfy the minimum requirements of fitting the RWBM with only two OGSE. Further investigation with multiple OGSE will help us to understand the behavior of the RWBM. Third, OGSE is a prototype sequence, which is not used in clinical scan. This sequence requires additional settings. Nevertheless, the RWBM yields parameters beyond analyzing DW images with a single diffusion time and has potential to reveal microstructure of brain tumors with further investigation.

Chapter 6 Conclusion, Summary, and Implication

This work investigated three dimensions of the parameter space for high-order diffusion models of DWI: b-value, TE, and diffusion time. Using different combinations of the three dimensions, we investigated a total of four high-order diffusion models, which revealed important pathological and derived computational features in GBM. The implications of these models will be discussed in the following aspects: minimal hardware requirements, diffusion data requirements for parameter fitting, stability of the models, ability to reveal features in GBM, and clinical utility of the derived parameters.

Chapter 2 described the work that modeled the diffusion effects using a microstructure model including intracellular and extracellular components. In this chapter, the microstructure model was modulated with a bipolar pulse diffusion gradient imaging modality and applied to characterize microstructure and diffusion properties of hyper-cellular tumors in patients with GBM. The microstructure model was able to differentiate GBM and normal tissue and has great potential to supplement conventional MRI in GBM diagnosis. Our microstructure model could be performed with a PGSE that is widely available on clinical scanners. We fitted the microstructure model with diffusion data from 11 subjects using high b-values up to 2500 s/mm^2. The b-values were chosen according to the availability on clinical MRI machines. However, we found that the microstructure model does not guarantee stability in voxel fitting. The model is complex and non-convex (Eq. A5), which may have contributed to the instability, although only having four parameters were used in the model. Additional contributors to the instability may

include low SNR in the high b-value DWI since we have applied four b-values that are greater than 1500 s/mm^2. The modeled microstructure yielded a radius that we could compare to an existing pathological research [59] in GBM, but our estimated cell diameter is substantially larger than the reported cell sizes. The larger computed radius may be caused our choice of modeling the cell boundaries to be impermeable to water, which may have artificially increased cell sizes due to restricted water diffusion across cell membranes. Additionally, the low SNR in DW images could further cause an overestimate of R. The estimated cell diameter may help physicians to diagnose GBM better together with the estimated D_{ex} and V_{in}.

Chapter 3 investigated the non-Gaussian water diffusion behavior in GBM. In Chapter 3, we studied the diffusion kurtosis model and characterized non-Gaussian diffusion properties in the Gd-GTVs pre-RT and mid-RT in patients with GBM. In our analysis, the DKI could be performed by PGSE with b-values less than 11, while higher b-values would influence kurtosis. Kurtosis calculated from higher b-values decreased by less than 10% compared with kurtosis calculated from lower b-values. To compensate the low SNR in the DWI, we first applied a Gaussian filter to the brain images and then generated voxel-wised parameter maps with DKI. The kurtosis from the DKI showed agreement with previous research in glioma grading [29,32,36], and high value of kurtosis is correlated with inferior survival. However, there are two problems of the DKI. Direct correlations between kurtosis and pathological features in GBM is difficult to find, and clear edges of tumor regions could not be seen on a kurtosis map (see Figure 3-2). Nonetheless, higher mean kurtosis values are found to correlate with inferior patient survival

rates. The kurtosis map may provide physicians with more information in tumor progression to adjust the aggressiveness in radiation therapy.

Chapter 4 explored a simplified T2-relaxation-diffusion correlation that combined TE space and b-value space together. In this study, we simplified the model of Bernin et al. [16] to fit the DW images and characterize diffusion properties of the hyper-cellular tumor in the patients with GBM. The simplified T2-relaxation-diffusion correlation showed that different DC values can have different T2 values. We have discussed the details in Chapter 4 how different TEs will influence DC values in mono- and bi-exponential models. Parameters estimated from T2-relaxation-diffusion model have the potential to identify GBM and some parameters, such as $T2_f$ and V_s, correlated with PFS and show potentials to predict survival. The T2-relaxation diffusion correlation could be performed with PGSE, but diffusion data with multiple TEs were required, requiring more data collection. To fit the six optimal parameters in our T2-relaxation-diffusion model, we applied diffusion data from 11 subjects at two TEs. Two sets of DWI required more scanning time. For the T2-relaxation-diffusion model, we could only perform analysis in VOI. Fitting in voxels was made difficult by low SNR in the DWI. Suboptimal image registration results between the two TEs could lead to non-realistic results. Non-realistic results could also be seen in VOIs close to edges, cavity, and CSF. The estimated T2 of GBM was close to a previous study investigating T2 in grade III glioma [87], but studies in GBM are very limited. The T2 and V_s may aid into the diagnosis and prognosis of GBM.

Chapter 5 investigated the RWBM in the dimension of diffusion time. In this study, we tested the model of Novikov et al. [27] to fit the DW images with PGSE and two OGSE and

characterize microstructure and diffusion properties of the brain tumors in patients. In analysis of the RWBM, we found that the estimated tumor diameter is close to a previous study [59], but the estimated axon diameter and length were substantially different from reported values in literature [85,86]. The RWBM is promising in revealing GBM pathological features, but this modality requires high gradient performance, which is not common on clinical scanners. OGSE is a prototype diffusion sequence that is usually restricted to research settings. To perform the RWBM, a minimum of two OGSE and one PGSE sequences need to be applied in scanning, which increased total scanning time. In our study, we collected 19 diffusion data from all 10 patients to fit the RWBM. The RWBM with 4 parameters was stable in the fitting process. After applying a Gaussian filter to the brain images, parameter maps were almost universally stable except some edge voxels. The estimated cell diameter of the tumor cells from the RWBM was close to a published work [59], but our model was not able to estimate the length and diameter of axons due to hardware restrictions. A high-frequency OGSE that is beyond the capability of our scanner should be applied if the axon diameter (~ 2 μm) needs to be estimated, and a very long TE that exceeds WM T2 needs to be applied if we investigate the length of an axon (over 100 μm). However, our accurate estimations of the tumor cell diameter could aid diagnosis and prognosis for GBM, and the estimated membrane permeability could also help physicians with further pathological validation. Overall, the RWBM is more promising than the other three models to help identify physiological features of GBM.

From the discussion above, all the four models revealed some features of GBM with potential diagnostic value that were not reported by conventional MRI. Among the four models,

RWBM could directly reveal several pathological features of GBM and showed a stable fit in voxels. The RWBM could be a promising model with additional investigation. Further study could include optimization that minimizing the b-values used in scan and optimize the frequency of OGSE to decrease the scanning time.

In summary, this work investigated four high-order diffusion models in all three dimensions of the parameter space that could be explored in diffusion MRI. These high-order diffusion models possess potential value for GBM that may be beneficial for diagnosis and prognosis for GBM in clinics, while the derived parameters could provide insight to plans for radiation therapy.

Appendix
The Equations of S_{in} for Three Bi-polar Diffusion Gradient Waveforms

In the first diffusion gradient waveform shown in Figure 2-1 and initially proposed by Fordham et.al [53], symmetric bi-polar diffusion gradients are placed before and after the 180° RF pulse. The gradient function can be expressed as:

$$g(t) = \begin{cases} g, & 0 < x < \delta \\ -g, & \delta < x < 2\delta \\ g, & \Delta < x < \Delta + \delta \\ -g, & \Delta + \delta < x < \Delta + 2\delta \end{cases} \quad \text{[A1]}$$

where g and δ are the magnitude and duration of diffusion gradient pulses, respectively, and Δ is the time interval between the gradient pulses before and after the 180° RF pulse. Note that the diffusion gradient pulse duration is the same for all positive and negative polar gradient pulses. This gradient waveform yields S_{in} in Eq 2.2 as:

$$S_{in} = exp\left(\left(\frac{\gamma g}{D_{in}}\right)^2 \sum_{i=1}^{n} \frac{B_n}{{\lambda_n}^2}\{-12 + 8D_{in}\lambda_n\delta + 16exp(-D_{in}\lambda_n\delta) - 4exp(-2D_{in}\lambda_n\delta) - 12exp(-D_{in}\lambda_n\Delta) + 16exp(-D_{in}\lambda_n\Delta)cosh(D_{in}\lambda_n\delta) - 4exp(-D_{in}\lambda_n\Delta)cosh(2D_{in}\lambda_n\delta)\}\right) \quad \text{[A2]}$$

where $\lambda_n$and B_n are the geometric factors related to the shape of cells [45], D_{in} is the intracellular diffusion coefficient, γ is the gyromagnetic ratio. The b-value of the diffusion pulse sequence is given by

$$b = \frac{4}{3}(\gamma g)^2\delta^3 \quad \text{[A3]}$$

In the second diffusion gradient waveform in Figure 2-1, four gradient pulses are placed before, after and between two 180° RF pulses. Pulse durations and separations can be tuned to minimize eddy currents for a system. Therefore, all four gradient pulse durations (δ_i) and time intervals between the pulses (Δ_i) can be different. A general waveform g(t) is described as:

$$g(t) = \begin{cases} g, & 0 < x < \delta_1 \\ g, & \Delta_1 < x < \Delta_1 + \delta_2 \\ -g, & \Delta_2 < x < \Delta_2 + \delta_3 \\ -g, & \Delta_3 < x < \Delta_3 + \delta_4 \end{cases}$$

and $\delta_1 + \delta_2 = \delta_3 + \delta_4$ [A4]

where δ_i is the i^{th} gradient pulse duration, and Δ_i is the time interval between the first and *i-1* pulse gradients (see Figure 2-1). This bi-polar diffusion gradient waveform results in S_{in} as:

$$S_{in}=\exp\left(\left(\frac{\gamma g}{D_{in}}\right)^2 \sum_{i=1}^{n} \frac{B_n}{\lambda_n{}^2}\{-8 + 2Din\lambda_n \sum_{i=1}^{4} \delta_i + 2\sum_{i=1}^{4} \exp(-D_{in}\lambda_n\delta_i) + 2(1 - \exp(D_{in}\lambda_n\delta_1))[-\exp(-D_{in}\lambda_n\Delta_1)(1-\exp(-D_{in}\lambda_n\delta_2)) + \exp(-D_{in}\lambda_n\Delta_2)(1-\exp(-D_{in}\lambda_n\delta_3)) + \exp(-D_{in}\lambda_n\Delta_3)(1-\exp(-D_{in}\lambda_n\delta_4))] + 2(1 - \exp(D_{in}\lambda_n\delta_2))[\exp(-D_{in}\lambda_n(\Delta_2 - \Delta_1))(1-\exp(-D_{in}\lambda_n\delta_3)) + \exp(-D_{in}\lambda_n(\Delta_3 - \Delta_1))(1-\exp(-D_{in}\lambda_n\delta_4))] + 2(1 - \exp(D_{in}\lambda_n\delta_3))\exp(-D_{in}\lambda_n(\Delta_3 - \Delta_2))(\cosh(D_{in}\lambda_n\delta_4)-1)\})$$ [A5]

The corresponding b-value is given by:

$$b = (\gamma g)^2[\tfrac{2}{3}(\delta_1 + \delta_2)^3 + \delta_1{}^2\tau_1 + (\delta_1 + \delta_2)^2\tau_2 + \delta_4{}^2\tau_3]$$ [A6]

where $\tau_1 = \Delta_1 - \delta_1$, $\tau_2 = \Delta_2 - \Delta_1 - \delta_2$, and $\tau_3 = \Delta_3 - \Delta_2 - \delta_3$.

In a special case of the second waveform, *g(t)* is described as:

$$g(t) = \begin{cases} g, & 0 < x < \delta \\ g, & \Delta < x < \Delta + \delta \\ -g, & 2\Delta < x < 2\Delta + \delta \\ -g, & 3\Delta < x < 3\Delta + \delta \end{cases} \quad \text{[A7]}$$

in which all diffusion gradient pulse durations are the same, and the gradient pulses are placed symmetrically related to the two 180° RF pulses. S_{in} is given as:

$$S_{in}=exp\left(\left(\frac{\gamma g}{D_{in}}\right)^2 \sum_{i=1}^{n} \frac{B_n}{{\lambda_n}^2}\{-8 + 8D_{in}\lambda_n\delta + 8exp(-D_{in}\lambda_n\delta) + 2\big(1 - exp(D_{in}\lambda_n\delta)\big)exp(-D_{in}\lambda_n\Delta)\big[\big(1 - exp(-D_{in}\lambda_n\delta)\big)\big(2exp(-D_{in}\lambda_n\Delta) + exp(-2D_{in}\lambda_n\Delta)\big) + cosh(D_{in}\lambda_n\delta) - 1\big]\}\right) \quad \text{[A8]}$$

The b-value is given by:

$$b = (\gamma g)^2 6\delta^2[\Delta - \tfrac{1}{9}\delta] \quad \text{[A9]}$$

References

1. Stupp R, Mason WP, van den Bent MJ, et al. Radiotherapy plus concomitant and adjuvant temozolomide for glioblastoma. *N Engl J Med.* 2005;352(10):987-996.
2. Prados MD, Chang SM, Butowski N, et al. Phase II study of erlotinib plus temozolomide during and after radiation therapy in patients with newly diagnosed glioblastoma multiforme or gliosarcoma. *J Clin Oncol.* 2009;27(4):579-584.
3. Wen PY, Macdonald DR, Reardon DA, et al. Updated response assessment criteria for high-grade gliomas: response assessment in neuro-oncology working group. *J Clin Oncol.* 2010;28(11):1963-1972.
4. Chenevert TL, Stegman LD, Taylor JMG, et al. Diffusion magnetic resonance imaging: an early surrogate marker of therapeutic efficacy in brain tumors. *J Natl Cancer I.* 2000;92(24):2029-2036.
5. Guo AC, Cummings TJ, Dash RC, Provenzale JM. Lymphomas and high-grade astrocytomas: Comparison of water diffusibility and histologic characteristics. *Radiology.* 2002;224(1):177-183.
6. Lyng H, Haraldseth O, Rofstad EK. Measurement of cell density and necrotic fraction in human melanoma xenografts by diffusion weighted magnetic resonance imaging. *Magn Reson Med.* 2000;43(6):828-836.
7. Sugahara T, Korogi Y, Kochi M, et al. Usefulness of diffusion-weighted MRI with echo-planar technique in the evaluation of cellularity in gliomas. *Jmri-J Magn Reson Im.* 1999;9(1):53-60.
8. Niendorf T, Dijkhuizen RM, Norris DG, Campagne MV, Nicolay K. Biexponential diffusion attenuation in various states of brain tissue: Implications for diffusion-weighted imaging. *Magn Reson Med.* 1996;36(6):847-857.
9. Maier SE, Bogner P, Bajzik G, et al. Normal brain and brain tumor: multicomponent apparent diffusion coefficient line scan imaging. *Radiology.* 2001;219(3):842-849.
10. Mulkern RV, Zengingonul HP, Robertson RL, et al. Multi-component apparent diffusion coefficients in human brain: relationship to spin-lattice relaxation. *Magn Reson Med.* 2000;44(2):292-300.
11. Jiang X, Li H, Xie J, et al. In vivo imaging of cancer cell size and cellularity using temporal diffusion spectroscopy. *Magn Reson Med.* 2017;78(1):156-164.
12. Jiang X, Li H, Xie J, Zhao P, Gore JC, Xu J. Quantification of cell size using temporal diffusion spectroscopy. *Magn Reson Med.* 2016;75(3):1076-1085.
13. Jiang X, Li H, Zhao P, et al. Early Detection of Treatment-Induced Mitotic Arrest Using Temporal Diffusion Magnetic Resonance Spectroscopy. *Neoplasia.* 2016;18(6):387-397.

14. Panagiotaki E, Walker-Samuel S, Siow B, et al. Noninvasive quantification of solid tumor microstructure using VERDICT MRI. *Cancer Res.* 2014;74(7):1902-1912.
15. Sui Y, Wang H, Liu G, et al. Differentiation of Low- and High-Grade Pediatric Brain Tumors with High b-Value Diffusion-weighted MR Imaging and a Fractional Order Calculus Model. *Radiology.* 2015;277(2):489-496.
16. Bernin D, Topgaard D. NMR diffusion and relaxation correlation methods: New insights in heterogeneous materials. *Curr Opin Colloid In.* 2013;18(3):166-172.
17. English AE, Whittall KP, Joy ML, Henkelman RM. Quantitative two-dimensional time correlation relaxometry. *Magn Reson Med.* 1991;22(2):425-434.
18. MacKay A, Whittall K, Adler J, Li D, Paty D, Graeb D. In vivo visualization of myelin water in brain by magnetic resonance. *Magn Reson Med.* 1994;31(6):673-677.
19. Schad LR, Brix G, Zuna I, Harle W, Lorenz WJ, Semmler W. Multiexponential proton spin-spin relaxation in MR imaging of human brain tumors. *J Comput Assist Tomogr*. 1989;13(4):577-587.
20. Seland JG, Bruvold M, Anthonsen H, et al. Determination of water compartments in rat myocardium using combined D-T1 and T1-T2 experiments. *Magn Reson Imaging.* 2005;23(2):353-354.
21. Seland JG, Bruvold M, Brurok H, Jynge P, Krane J. Analyzing equilibrium water exchange between myocardial tissue compartments using dynamical two-dimensional correlation experiments combined with manganese-enhanced relaxography. *Magn Reson Med.* 2007;58(4):674-686.
22. Istratov AA, Vyvenko OF. Exponential analysis in physical phenomena. *Rev Sci Instrum.* 1999;70(2):1233-1257.
23. Mitchell J, Chandrasekera TC, Gladden LF. Numerical estimation of relaxation and diffusion distributions in two dimensions. *Prog Nucl Magn Reson Spectrosc.* 2012;62:34-50.
24. Lemberskiy G, Fieremans E, Veraart J, Deng FM, Rosenkrantz AB, Novikov DS. Characterization of prostate microstructure using water diffusion and NMR relaxation. *Front Phys.* 2018;6.
25. Lemberskiy G, Rosenkrantz AB, Veraart J, Taneja SS, Novikov DS, Fieremans E. Time-Dependent Diffusion in Prostate Cancer. *Invest Radiol.* 2017;52(7):405-411.
26. Mitra PP, Sen PN, Schwartz LM. Short-time behavior of the diffusion coefficient as a geometrical probe of porous media. *Phys Rev B Condens Matter.* 1993;47(14):8565-8574.
27. Novikov DS, Fieremans E, Jensen JH, Helpern JA. Random walk with barriers. *Nat Phys.* 2011;7(6):508-514.
28. Veliz I, Loo Y, Castillo O, Karachaliou N, Nigro O, Rosell R. Advances and challenges in the molecular biology and treatment of glioblastoma-is there any hope for the future? *Ann Transl Med.* 2015;3(1):7.

29. Bai Y, Lin Y, Tian J, et al. Grading of Gliomas by Using Monoexponential, Biexponential, and Stretched Exponential Diffusion-weighted MR Imaging and Diffusion Kurtosis MR Imaging. *Radiology.* 2016;278(2):496-504.
30. Higano S, Yun X, Kumabe T, et al. Malignant astrocytic tumors: clinical importance of apparent diffusion coefficient in prediction of grade and prognosis. *Radiology.* 2006;241(3):839-846.
31. Law M, Young RJ, Babb JS, et al. Gliomas: predicting time to progression or survival with cerebral blood volume measurements at dynamic susceptibility-weighted contrast-enhanced perfusion MR imaging. *Radiology.* 2008;247(2):490-498.
32. Van Cauter S, Veraart J, Sijbers J, et al. Gliomas: diffusion kurtosis MR imaging in grading. *Radiology.* 2012;263(2):492-501.
33. Callaghan PT. Pulsed-gradient spin-echo NMR for planar, cylindrical and spherical pores under conditions of wall relaxation. *J Magn Reson.* 1995;113:53-59.
34. Neuman CH. Spin-Echo of Spins Diffusing in a Bounded Medium. *Journal of Chemical Physics.* 1974;60(11):4508-4511.
35. Stepisnik J. Time-dependent self-diffusion by NMR spin echo. *Physica B.* 1993;183:343-350.
36. Raab P, Hattingen E, Franz K, Zanella FE, Lanfermann H. Cerebral gliomas: diffusional kurtosis imaging analysis of microstructural differences. *Radiology.* 2010;254(3):876-881.
37. Hurlimann MD, Helmer KG, Deswiet TM, Sen PN. Spin Echoes in a Constant Gradient and in the Presence of Simple Restriction. *J Magn Reson Ser A.* 1995;113(2):260-264.
38. Li Y, Kim M, Lawrence TS, Parmar H, Cao Y. Microstructure Modeling of High b-Value Diffusion-Weighted Images in Glioblastoma. *Tomography.* 2020;6(1):34-43.
39. Kwee TC, Galban CJ, Tsien C, et al. Intravoxel water diffusion heterogeneity imaging of human high-grade gliomas. *NMR Biomed.* 2010;23(2):179-187.
40. Mardor Y, Pfeffer R, Spiegelmann R, et al. Early detection of response to radiation therapy in patients with brain malignancies using conventional and high b-value diffusion-weighted magnetic resonance imaging. *J Clin Oncol.* 2003;21(6):1094-1100.
41. Szczepankiewicz F, van Westen D, Englund E, et al. The link between diffusion MRI and tumor heterogeneity: Mapping cell eccentricity and density by diffusional variance decomposition (DIVIDE). *Neuroimage.* 2016;142:522-532.
42. White NS, McDonald CR, Farid N, Kuperman JM, Kesari S, Dale AM. Improved conspicuity and delineation of high-grade primary and metastatic brain tumors using "restriction spectrum imaging": quantitative comparison with high B-value DWI and ADC. *AJNR Am J Neuroradiol.* 2013;34(5):958-964, S951.
43. Reynaud O, Winters KV, Hoang DM, Wadghiri YZ, Novikov DS, Kim SG. Pulsed and oscillating gradient MRI for assessment of cell size and extracellular space (POMACE) in mouse gliomas. *NMR Biomed.* 2016;29(10):1350-1363.

44. Tian X, Li H, Jiang X, Xie J, Gore JC, Xu J. Evaluation and comparison of diffusion MR methods for measuring apparent transcytolemmal water exchange rate constant. *J Magn Reson.* 2017;275:29-37.
45. Xu J, Does MD, Gore JC. Quantitative characterization of tissue microstructure with temporal diffusion spectroscopy. *J Magn Reson.* 2009;200(2):189-197.
46. Xu J, Does MD, Gore JC. Sensitivity of MR diffusion measurements to variations in intracellular structure: effects of nuclear size. *Magn Reson Med.* 2009;61(4):828-833.
47. Pramanik PP, Parmar HA, Mammoser AG, et al. Hypercellularity Components of Glioblastoma Identified by High b-Value Diffusion-Weighted Imaging. *Int J Radiat Oncol.* 2015;92(4):811-819.
48. Wahl DR, Kim MM, Aryal MP, et al. Combining Perfusion and High B-value Diffusion MRI to Inform Prognosis and Predict Failure Patterns in Glioblastoma. *Int J Radiat Oncol Biol Phys.* 2018;102(4):757-764.
49. Kim MM, Parmar HA, Aryal MP, et al. Developing a Pipeline for Multiparametric MRI-Guided Radiation Therapy: Initial Results from a Phase II Clinical Trial in Newly Diagnosed Glioblastoma. *Tomography.* 2019;5(1):118-126.
50. Li K, Li H, Zhang XY, et al. Influence of water compartmentation and heterogeneous relaxation on quantitative magnetization transfer imaging in rodent brain tumors. *Magn Reson Med.* 2016;76(2):635-644.
51. Balinov B, Jonsson B, Linse P, Soderman O. The Nmr Self-Diffusion Method Applied to Restricted Diffusion - Simulation of Echo Attenuation from Molecules in Spheres and between Planes (Vol 104, Pg 17, 1993). *J Magn Reson Ser A.* 1994;108(1):130-130.
52. Reese TG, Heid O, Weisskoff RM, Wedeen VJ. Reduction of eddy-current-induced distortion in diffusion MRI using a twice-refocused spin echo. *Magn Reson Med.* 2003;49(1):177-182.
53. Fordham EJ, Hall LD, Ramakrishnan TS, Sharpe MR, Hall C. Saturation Gradients in Drainage of Porous-Media - Nmr Imaging Measurements. *Aiche Journal.* 1993;39(9):1431-1443.
54. Issa B. In vivo measurement of the apparent diffusion coefficient in normal and malignant prostatic tissues using echo-planar imaging. *Journal of Magnetic Resonance Imaging.* 2002;16(2):196-200.
55. Field AS, Alexander AL. Diffusion tensor imaging in cerebral tumor diagnosis and therapy. *Top Magn Reson Imaging.* 2004;15(5):315-324.
56. LaViolette PS, Mickevicius NJ, Cochran EJ, et al. Precise ex vivo histological validation of heightened cellularity and diffusion-restricted necrosis in regions of dark apparent diffusion coefficient in 7 cases of high-grade glioma. *Neuro-Oncology.* 2014;16(12):1599-1606.
57. Nafe R, Franz K, Schlote W, Schneider B. Morphology of tumor cell nuclei is significantly related with survival time of patients with glioblastomas. *Clinical Cancer Research.* 2005;11(6):2141-2148.

58. Dietrich O, Raya JG, Reeder SB, Reiser MF, Schoenberg SO. Measurement of signal-to-noise ratios in MR images: influence of multichannel coils, parallel imaging, and reconstruction filters. *J Magn Reson Imaging.* 2007;26(2):375-385.
59. Eidel O, Neumann JO, Burth S, et al. Automatic Analysis of Cellularity in Glioblastoma and Correlation with ADC Using Trajectory Analysis and Automatic Nuclei Counting. *PLoS One.* 2016;11(7):e0160250.
60. Li H, Jiang X, Xie J, Gore JC, Xu J. Impact of transcytolemmal water exchange on estimates of tissue microstructural properties derived from diffusion MRI. *Magn Reson Med.* 2017;77(6):2239-2249.
61. Chang EL, Akyurek S, Avalos T, et al. Evaluation of peritumoral edema in the delineation of radiotherapy clinical target volumes for glioblastoma. *Int J Radiat Oncol Biol Phys.* 2007;68(1):144-150.
62. Kelly PJ, Daumas-Duport C, Kispert DB, Kall BA, Scheithauer BW, Illig JJ. Imaging-based stereotaxic serial biopsies in untreated intracranial glial neoplasms. *J Neurosurg.* 1987;66(6):865-874.
63. Lebihan D, Breton E, Lallemand D, Aubin ML, Vignaud J, Lavaljeantet M. Separation of Diffusion and Perfusion in Intravoxel Incoherent Motion Mr Imaging. *Radiology.* 1988;168(2):497-505.
64. Li Y, Kim MM, Wahl DR, Lawrence TS, Parmar H, Cao Y. Survival Prediction Analysis in Glioblastoma With Diffusion Kurtosis Imaging. 2021;11(2695).
65. Wu EX, Cheung MM. MR diffusion kurtosis imaging for neural tissue characterization. *NMR Biomed.* 2010;23(7):836-848.
66. Zhang J, Jiang J, Zhao L, et al. Survival prediction of high-grade glioma patients with diffusion kurtosis imaging. *Am J Transl Res.* 2019;11(6):3680-3688.
67. Kim MM, Sun Y, Aryal MP, et al. A Phase II Study of Dose-Intensified Chemoradiation Using Biologically-Based Target Volume Definition in Patients with Newly Diagnosed Glioblastoma. *Int J Radiat Oncol.* 2020;108(3):S20-S20.
68. Jensen JH, Helpern JA. MRI quantification of non-Gaussian water diffusion by kurtosis analysis. *Nmr in Biomedicine.* 2010;23(7):698-710.
69. Cui Y, Ma L, Chen X, Zhang Z, Jiang H, Lin S. Lower apparent diffusion coefficients indicate distinct prognosis in low-grade and high-grade glioma. *J Neurooncol.* 2014;119(2):377-385.
70. Murakami R, Sugahara T, Nakamura H, et al. Malignant supratentorial astrocytoma treated with postoperative radiation therapy: prognostic value of pretreatment quantitative diffusion-weighted MR imaging. *Radiology.* 2007;243(2):493-499.
71. Yamasaki F, Sugiyama K, Ohtaki M, et al. Glioblastoma treated with postoperative radiochemotherapy: prognostic value of apparent diffusion coefficient at MR imaging. *Eur J Radiol.* 2010;73(3):532-537.
72. Zulfiqar M, Yousem DM, Lai H. ADC values and prognosis of malignant astrocytomas: does lower ADC predict a worse prognosis independent of grade of tumor?--a meta-analysis. *AJR Am J Roentgenol.* 2013;200(3):624-629.

73. Sehy JV, Ackerman JJ, Neil JJ. Evidence that both fast and slow water ADC components arise from intracellular space. *Magn Reson Med.* 2002;48(5):765-770.
74. Sehy JV, Zhao L, Xu J, Rayala HJ, Ackerman JJ, Neil JJ. Effects of physiologic challenge on the ADC of intracellular water in the Xenopus oocyte. *Magn Reson Med.* 2004;52(2):239-247.
75. Hempel JM, Brendle C, Bender B, et al. Diffusion kurtosis imaging histogram parameter metrics predicting survival in integrated molecular subtypes of diffuse glioma: An observational cohort study. *Eur J Radiol.* 2019;112:144-152.
76. Matsusue E, Fink JR, Rockhill JK, Ogawa T, Maravilla KR. Distinction between glioma progression and post-radiation change by combined physiologic MR imaging. *Neuroradiology.* 2010;52(4):297-306.
77. Li Y, Kim M, Lawrence TS, Parmar H, Cao Y. Analysis of the T2-relaxation-diffusion Correlation MRI in Glioblastoma. Paper presented at: ISMRM2018; Paris, France.
78. Li Y, Kim M, Lawrence TS, Parmar H, Cao Y. T2-Relaxation-Diffusion Correlation Analysis for Prediction of Progression Free Survival (PFS) in Glioblastoma. Paper presented at: AAPM2020; Virtual.
79. Wansapura JP, Holland SK, Dunn RS, Ball WS, Jr. NMR relaxation times in the human brain at 3.0 tesla. *J Magn Reson Imaging.* 1999;9(4):531-538.
80. Chou MC, Tsai PH, Huang GS, et al. Correlation between the MR T2 value at 4.7 T and relative water content in articular cartilage in experimental osteoarthritis induced by ACL transection. *Osteoarthr Cartilage.* 2009;17(4):441-447.
81. Li Y, Kim M, Lawrence TS, Feiweier T, Cao Y. Analysis of Diffusion and Microstructure Properties in Brain Tumors Using a Random Walk with Barriers Model. Paper presented at: AAPM2021; Virtual.
82. Rakow-Penner RA, White NS, Parsons JK, et al. Novel technique for characterizing prostate cancer utilizing MRI restriction spectrum imaging: proof of principle and initial clinical experience with extraprostatic extension. *Prostate Cancer Prostatic Dis.* 2015;18(1):81-85.
83. Reynaud O. Time-Dependent Diffusion MRI in Cancer: Tissue Modeling and Applications. *Frontiers in Physics.* 2017;5.
84. Deswiet TM, Sen PN. Decay of Nuclear Magnetization by Bounded Diffusion in a Constant Field Gradient. *Journal of Chemical Physics.* 1994;100(8):5597-5604.
85. Arnold N, Harriman DG. The incidence of abnormality in control human peripheral nerves studied by single axon dissection. *J Neurol Neurosurg Psychiatry.* 1970;33(1):55-61.
86. Friede RL, Bischhausen R. How Are Sheath Dimensions Affected by Axon Caliber and Internode Length. *Brain Res.* 1982;235(2):335-350.
87. Kern M, Auer TA, Picht T, Misch M, Wiener E. T2 mapping of molecular subtypes of WHO grade II/III gliomas. *BMC Neurol.* 2020;20(1):8.